NAVAL POSTGRADUATE SCHOOL

MONTEREY, CALIFORNIA

DISSERTATION

WAVE TRANSFORMATION ON A ROCKY SHORELINE

by

Casey J. Gon

September 2019

Dissertation Supervisor: James H. MacMahan

Approved for public release. Distribution is unlimited.

THIS PAGE INTENTIONALLY LEFT BLANK

REPORT DOCUMENTATION PAGE			*Form Approved OMB No. 0704-0188*

1. AGENCY USE ONLY *(Leave blank)*	**2. REPORT DATE** September 2019	**3. REPORT TYPE AND DATES COVERED** Dissertation

4. TITLE AND SUBTITLE WAVE TRANSFORMATION ON A ROCKY SHORELINE	**5. FUNDING NUMBERS** RQMV2
6. AUTHOR(S) Casey J. Gon	
7. PERFORMING ORGANIZATION NAME(S) AND ADDRESS(ES) Naval Postgraduate School Monterey, CA 93943-5000	**8. PERFORMING ORGANIZATION REPORT NUMBER**
9. SPONSORING / MONITORING AGENCY NAME(S) AND ADDRESS(ES) Office of Naval Research, Arlington, VA, 22203	**10. SPONSORING / MONITORING AGENCY REPORT NUMBER**

11. SUPPLEMENTARY NOTES The views expressed in this thesis are those of the author and do not reflect the official policy or position of the Department of Defense or the U.S. Government.

12a. DISTRIBUTION / AVAILABILITY STATEMENT Approved for public release. Distribution is unlimited.	**12b. DISTRIBUTION CODE** A

13. ABSTRACT (maximum 200 words)

Two month-long experiments were performed to evaluate wave transformation across a rough rocky reef at Hopkins Marine Station, Monterey Bay, California. Outside of wave breaking, approximately 30% of the measured wave energy flux by sea and swell waves was dissipated over 140m. The bottom roughness of the rocky reef is defined by the standard deviation of bottom vertical variability (σ_b) and is 0.9 m. The energy dissipation, $\langle \varepsilon_f \rangle$, is related to bottom friction resulting in energy friction factor (fe) found to range between 0.03 and 43.8. An empirical power-law relationship was developed for fe as a function of wave orbital excursion (Ab) and σ_b. Inside of wave breaking at the shallow-water stations (h<2 m), wave heights, Hrms, collapsed to a non-linear relationship as a function of h that was lower than the estimated wave breaking parameter for this site, γ=0.29. An analytical model for shallow-water wave transformation on a plane sloping bottom with bottom friction only was derived matching the observed results. In deeper stations (h>2m), wave transformation is due to a combination of friction and wave breaking. Field-estimated fe ranged 3.8–8.2. These parameters were applied within the Thornton and Guza wave transformation model from 1983, and tested across the measurement array resulting in skill $\geq$ 0.9. The wave response to being frictionally dominant has important implications in describing biological communities within a rocky environment.

14. SUBJECT TERMS wave energy dissipation, bottom friction, rocky reef, wave transformation, wave breaking parameter, gamma	**15. NUMBER OF PAGES** 67
	16. PRICE CODE

17. SECURITY CLASSIFICATION OF REPORT	**18. SECURITY CLASSIFICATION OF THIS PAGE**	**19. SECURITY CLASSIFICATION OF ABSTRACT**	**20. LIMITATION OF ABSTRACT**
Unclassified	Unclassified	Unclassified	UU

NSN 7540-01-280-5500 Standard Form 298 (Rev. 2-89)
Prescribed by ANSI Std. 239-18

THIS PAGE INTENTIONALLY LEFT BLANK

Approved for public release. Distribution is unlimited.

WAVE TRANSFORMATION ON A ROCKY SHORELINE

Casey J. Gon
Commander, United States Navy
BS, U.S. Naval Academy, 2003
MBA, Salve Regina College, 2009
MS, Naval Postgraduate School, 2013

Submitted in partial fulfillment of the
requirements for the degree of

DOCTOR OF PHILOSOPHY IN PHYSICAL OCEANOGRAPHY

from the

NAVAL POSTGRADUATE SCHOOL
September 2019

Approved by:

James H. MacMahan
Department of Oceanography
Dissertation Supervisor

Wendell A. Nuss
Department of Meteorology

Derek Olson
Department of Oceanography

Mara S. Orescanin
Department of Oceanography

Edward B. Thornton
Department of Oceanography

Mark Denny
Stanford Hopkins Marine Station

James H. MacMahan
Department of Oceanography
Dissertation Chair

Approved by:

Peter C. Chu
Chair, Department of Oceanography

Orrin D. Moses
Vice Provost of Academic Affairs

THIS PAGE INTENTIONALLY LEFT BLANK

ABSTRACT

Two month-long experiments were performed to evaluate wave transformation across a rough rocky reef at Hopkins Marine Station, Monterey Bay, California. Outside of wave breaking, approximately 30% of the measured wave energy flux by sea and swell waves was dissipated over 140m. The bottom roughness of the rocky reef is defined by the standard deviation of bottom vertical variability (σ_b) and is 0.9 m. The energy dissipation, $\langle \varepsilon_f \rangle$, is related to bottom friction resulting in energy friction factor (fe) found to range between 0.03 and 43.8. An empirical power-law relationship was developed for fe as a function of wave orbital excursion (Ab) and σ_b. Inside of wave breaking at the shallow-water stations ($h<2$ m), wave heights, Hrms, collapsed to a non-linear relationship as a function of h that was lower than the estimated wave breaking parameter for this site, $\gamma=0.29$. An analytical model for shallow-water wave transformation on a plane sloping bottom with bottom friction only was derived matching the observed results. In deeper stations ($h>2$m), wave transformation is due to a combination of friction and wave breaking. Field-estimated fe ranged 3.8–8.2. These parameters were applied within the Thornton and Guza wave transformation model from 1983, and tested across the measurement array resulting in skill ≥ 0.9. The wave response to being frictionally dominant has important implications in describing biological communities within a rocky environment.

THIS PAGE INTENTIONALLY LEFT BLANK

TABLE OF CONTENTS

I. INTRODUCTION....1

II. WAVE DISSIPATION BY BOTTOM FRICTION ON A ROUGH ROCKY REEF....5
- A. FIELD EXPERIMENT....5
- B. 3 METHODS....9
  - 1. Wave Estimates from Pressure....9
  - 2. Wave Estimates at the Edge of Reef (EOR)....9
  - 3. Dissipation....10
- C. RESULTS OF DISSIPATION DUE TO BOTTOM FRICTION....11
- D. DISCUSSION....13
  - 1. Bottom Roughness....13
  - 2. Midpoint Method for Energy Friction Factors....15
  - 3. Relating f_e to σb....17

III. NEARSHORE WAVE TRANSFORMATION OVER A ROCKY REEF SHORELINE....23
- A. FIELD EXPERIMENT....23
- B. DISSIPATION DUE TO WAVE BREAKING AND FRICTION....27
- C. RESULTS....30
  - 1. γ in the Breaking Zone and Wave Breaking Due to Friction in the Friction Zone....30
  - 2. Energy Coefficients, f_e....33
  - 3. Dissipation in the BZ and FZ....35
- D. DISCUSSION....36
  - 1. Dissipation by Wave Breaking and Friction....36
  - 2. Analytical Model with Bottom Friction Dissipation Only....37
  - 3. Model Skill of TG83 on a Rocky Reef....39

IV. CONCLUSIONS....41

LIST OF REFERENCES....45

INITIAL DISTRIBUTION LIST....51

THIS PAGE INTENTIONALLY LEFT BLANK

LIST OF FIGURES

Figure 1. Map of Monterey Bay and its corresponding bathymetry. 7

Figure 2. a and b) Time series of wave energy flux at the EOR (black line) compared to A and B (grey line) for experiment A and B; c and d) Time series of wave energy dissipation between EOR and A and B.....11

Figure 3. Time series of average H_{rms} between EOR and experiment A (a) and B (b); times series of f_e calculated from (7) for experiment A (c) and experiment B (d). 12

Figure 4. f_e as a function of mean A_b between the EOR and including data from experiment A and B. 13

Figure 5. Histogram of detrended vertical elevations (z') from Figure 1d. 14

Figure 6. 2D autocorrelation of the detrended bathymetry. 15

Figure 7. Scatter plot of $f_{e,midpoint}$ compared to f_e where the dot color represents T, which is color scaled to the right. 16

Figure 8. Bin-averaged f_e (symbols) plotted as a function of $A_b/\sigma b$, from multiple field experiments. 18

Figure 9. Picture from Stanford Hopkins Marine Station at low tide showing the irregularities of the rocky coastline.....24

Figure 10. Bathymetry and topography of HMS contoured in 1 m increments. 25

Figure 11. Instrument elevations and experimental mean H_{rms}.....26

Figure 12. Hrms as a function of h for experiment A. 31

Figure 13. Hrms as a function of h for experiment B.....32

Figure 14. f_e as a function of A_b for the BZ (grey circles) and the FZ (black circles).....34

Figure 15. a) F at BZ1 (black line) and BZ5 (grey line); b) F at FZ1 (black line) and FZ6 (grey line). 35

Figure 16. a and b) % reduction in F at BZ1 (FZ1) and BZ2 (FZ3) as a function of H_{rms} and tide; c and d) % contribution of εf (black dots) and εb(grey dots) to ε between BZ1 (FZ1) and BZ2 (FZ3) as a function of H_{rms}. 37

Figure 17. GTM model sensitivity analysis. 39

Figure 18. Model skill plotted as a function of tide and incident H_{rms} defined by the dot color. 40

LIST OF ACRONYMS AND ABBREVIATIONS

A	Experiment Site A
A_b	Wave Orbital Excursion
ADCP	Acoustic Doppler Current Profiler
B	Experiments Site B
BZ	Breaking Zone
C	Wave Phase Speed
C_g	Wave Group Speed
C_f	Bed Friction Coefficient
CPB	Cabrillo Point Buoy
CSUMB	California State University at Monterey Bay
D	Diameter
EOR	Edge of Reef
F	Energy Flux
f	Frequency
f_e	Wave Energy Friction Factor
$f_{e,midpoint}$	Wave Energy Friction Factor solved using Midpoint Method
f_w	Total Friction Factor
FZ	Friction Zone
g	Gravitational Constant
GTM	Gon Thornton MacMahan
h	Depth
H	Wave Height
Hz	Hertz
H_{rms}	Root Mean Square Wave Height
k	Wave Number
k_n	Geometric Roughness
L	Wavelength
m	Meter
MSL	Mean Seal Level

p_d	Dynamic Pressure
Q	Bore Discharge
R^2	Reflection Coefficient
RMSE	Root Mean Square Error
SFML	Seafloor Mapping Laboratory
s	Seconds
T	Period
TG83	Thornton and Guza (1983)
u_b	Bottom Orbital Velocity
x	Cross-shore
y	alongshore
z	elevation
z_o	Hydrodynamic Roughness
β	Proportionality Coefficient (Chapter II)
β	Bottom Slope (Chapter III)
γ	Wave Breaking Parameter
ε	Total Dissipation
ε_b	Dissipation due to Breaking
ε_f	Dissipation due to Bottom Friction
η	Sea Surface Elevation
θ	Wave Direction
ρ	Density of Seawater
σ^2	Variance
σ_b	Geometric Roughness based on Standard Deviation of Height Elements
τ_b	Bottom Shear Stress
ω	Radian Frequency

ACKNOWLEDGMENTS

I would like to express my sincere and heartfelt thanks to my advisor, Jamie MacMahan, for his patience and guidance and endless support over the past three years. You have challenged me to be my best self in the classroom, in the field, and outside of the classroom. You know when to push, when to pull, and when to give space. I am forever grateful for the life lessons I have learned from you. You are more than an advisor; you are a friend.

I would also like to give my genuine thanks to my co-advisor, Ed Thornton. Ed, your timing was always perfect. When I did not think I could do it, or did not understand, you came to the rescue. Thank you for your patience and mentorship. It was an honor to work with you and learn from one of the giants in the nearshore community.

To Dr. Mark Denny and the staff at Stanford: without your support, studying the rocky shoreline would not have been possible. The team at Stanford allowed the Rocky Shoreline Team to push the limits in the name of science. I am forever grateful and will miss my time at Hopkins Marine Station.

I would like to thank Keith Wyckoff. Keith, you always showed me how to do things the correct way. Without this guidance, I would have no idea how to work in the field. Your commitment and “can do” attitude is how we figured out how to work in this complex environment. You are more than a field mentor; you are a friend. Thank you for the life advice; NPS is lucky to have you.

Lastly, I would like to thank my family for their continual and absolute support. Mom, you are the rock of our family. Your constant encouragement and belief that I can do anything is not lost on me, and you managed to have these thoughts in the deepest and darkest days of this process. You are the reason this was possible, and you are the reason I am able to get up and persist.

THIS PAGE INTENTIONALLY LEFT BLANK

I. INTRODUCTION

It is estimated that 75 percent of the world's coastlines can be described as rocky (Bird 2000). Only a few wave transformation measurements have been made on rocky shorelines, and those studies have been limited to rocky shore platforms, which constitute about 20 percent of rocky shorelines (Kirk 1977; Emery and Kuhn 1982; Trenhaile 2002; Poate et al. 2018). Rocky shore platforms are classified as either a seaward sloping uniform ramp (type A) or near horizontal with an abrupt cliff at the seaward extent (type B) (Sunamura 1992; Kennedy and Beban 2005; Marshall and Stephenson 2011). The rest of rocky shorelines can be characterized as "rougher," and are commonly studied by marine biologists owing to their diverse complexity in colony structure, and high density of marine biota (Denny et al. 1992; Koehl and Powell 1994; Trowbridge 2004). "Rougher" rocky shorelines will be referred to as rocky reefs. The rocky reef-like structure supports a quasi-random undulation of rock mounds that results in quick transitions, forming bathymetric highs and lows.

Several studies of wave transformation have been conducted over coral reefs whose seabed is rough (Lowe et al. 2005; Péquignet et al. 2011; Monismith et al. 2013; Monismith et al. 2015, Rogers et al. 2016; Lentz et al. 2016), and are included as a comparison with the measurements here. Unlike coral reefs, rocky reefs can extend well above the high-tide water line. The large bathymetric variability as it extends to the intertidal zone forms the commonly observed shallow-water tide pools, where the size of the pool depends on rocky relief (Storlazzi and Field 2000). The irregularity of rocky reef shorelines results in narrow, irregular wave-swept surge channels (Denny et al. 1992), to small coves, to larger pocket beaches (Storlazzi and Field 2000). Coral reefs are living organisms that biologically and hydrodynamically evolve (Monismith 2007) whereas rocky reefs are not living organisms, slowly erode, and can be considered a relatively static bottom. Rocky reefs also exist in meso- to macro-tidal environments and can be exposed to larger waves than most coral reefs, which are typically located in micro-tidal environments with smaller waves (Kench and Brander 2006). On a rocky reef in Monterey, CA, Denny et al. (2003) used dynamometers and measured impact velocities due to wave breaking on the rocks can

exceed 25 m/s. These impact velocities define the colony structure (Denny et al. 2003). The biological recruitment, migration, and transport for rocky reefs are critical in the health of the ecosystem, where waves are hypothesized to govern relevant processes.

To improve our understanding of waves on the rocky reef ecosystem, wave transformation across the rough bottom seaward of wave breaking is required. In Chapter II, wave energy flux (F), outside of wave breaking is defined by:

$$\frac{\partial EC_g}{\partial x} = \varepsilon_f, \tag{1}$$

where, E is the energy and $E = {}^{1}/_{8}\,\rho g H_{rms}^2$. C_g is the group wave speed represented by $C\ 1/2\left(1+\frac{2kh}{sinh2kh}\right)cos\theta$, where C is the wave phase speed, k is the wave number and $\theta$is the wave direction. x is positive in the direction of wave propagation and $\varepsilon_f$is dissipation due to bed friction. Seaward of the surf zone, outside of wave breaking, and assuming waves are approaching shore normal, over straight and parallel contours, changes in F are solely a function of the cross shore component (x) and are due to $\varepsilon_f$where:

$$\varepsilon_f = \overline{\tau_b u_b}, \tag{2}$$

the overbar indicates time averaging, $u_b$is the wave orbital velocity at the seabed and $\tau_b$is the bottom shear stress defined by (Jonsson 1966):

$$\tau_b = \frac{f_w}{2}\rho\overline{u_b|u_b|}, \tag{3}$$

where ρ is the density of seawater and f_w is the wave friction factor, which is related to the bed friction coefficient (C_f) by $f_w = 2C_f$. C_f or f_w are friction factors commonly described in the literature though with different nomenclatures defining f_w. For example, Dean and Dalrymple (1992) define τ_b using the Darcy-Wiesbach definition of $f_w/6$ (Fanning 1877), whereas Jonsson 1966 uses $f_w/2$.

For energy dissipation with τ_b described by (3), the relevant coefficient is changed to f_e, referred to as the energy friction factor. While mathematically f_w and f_e are not equivalent due to a phase shift between the τ_b and u_b,when both friction factors are compared to each other, large experimental scatter exists, and they are often assumed equal

(Nielsen 1992). Friction factors from this point forward will be referred to as f_e since the analysis is based on energy dissipation. The impact of ε_f based on f_e as a function of bottom roughness on the rocky reef is discussed.

On sandy beaches, f_e is 0.01-0.02 (Thornton and Guza 1986). Poate et al. (2018) found f_e to range from 0.04 to 0.14 on Type A rocky platforms. For rougher coral reef bottoms, Lowe et al. (2005) found f_e to be 0.28, while on very rough reefs Monismith et al. (2015) found f_e to be 1.86 and Lentz et al. (2016) found f_e to range from 0.9-4.2 depending on wave conditions. As bottom roughness increases, f_e is found to increase.

In Chapter III, the study of wave transformation on the rocky reef is continued inside of wave breaking. On sandy beaches inside of wave breaking, the wave height (H_{rms}) is found to linearly depend on water depth (h), such that

$$H_{rms} = \gamma h \tag{4}$$

where γ is the wave breaking parameter. This is referred to as depth-limited breaking and describes saturated conditions when all waves of the height distribution are breaking (Thornton and Guza 1983; hereafter TG83). A number of empirical relationships for sandy beaches have been developed for wave saturation relating γ to the offshore wave characteristics and/or beach slopes (Iversen 1952; Miche 1951 Sallenger and Hollman 1985; Masselink and Hegge 1995; Raubenheimer et al. 1996; Baldock et al. 1998; Ruessink et al. 2003). Wide ranges of γ are found on sandy beaches with a typical value of 0.4 based on TG83. Field observation of breaking waves heights on non-sandy beaches, such as rocky platforms and coral reefs, also vary linearly as in (4). For rocky platforms, Poate et al. (2018) found γ to be 0.29–0.46, which is similar to sandy beaches. For coral reefs, γ was found to be 0.07–0.85 (Harris et al. 2018) and 0.15–0.45 (Monosmith et al. 2013) while others found values 0.2–0.3 (Young 1989; Lowe et al. 2009; Harris and Vil-Concejo 2013). γ for coral reefs, particularly across the reef flats, can be lower than typically observed on sandy beaches, which is related to the increase in bottom friction owing to increased bottom roughness (Lentz et al. 2016; Harris et al. 2018). Lentz et al. (2016) observed for a flat bottom (i.e., the reef flat) that the depth-limited waves and correspondingly low γ were associated with bottom friction, not wave breaking after the initial onset of wave breaking

at the edge of the reef. This dominant frictional wave dissipation in shallow water resulted in a non-linear relationship between H_{rms} and h on the rocky reef. As seen outside of wave breaking, friction continues to be the dominant factor in wave transformation inside of wave breaking.

II. WAVE DISSIPATION BY BOTTOM FRICTION ON A ROUGH ROCKY REEF

The objective herein is to measure ε_f and determine f_e outside of the surf zone on a natural rocky reef. Wave measurements were collected on a rocky reef in Monterey Bay. Bottom rocky roughness represented as the standard deviation of the bathymetry (σ_b) is found to be 8–10 times larger than observed by Lowe et al. (2005) and Lentz et al. (2016) on coral reefs. f_e is evaluated with measured σ_b and wave orbital excursions, A_b and compared with other studies with ranging bottom roughness. Additionally, the discussion includes the relationship of average profile depth estimates in determining f_e. Finally, an empirical relationship between f_e and A_b based on σ_b and previous experiments are included. Owing to large roughness measurements compared to coral reefs, it is expected that ε_f will be an important contributing factor to the understanding of how the diverse biological colonies are able to thrive in such a dynamic environment.

A. FIELD EXPERIMENT

Surface gravity waves were measured by bottom-mounted pressure sensors deployed on the rocky reef off the coast of Stanford's Hopkins Marine Station, Monterey Bay, California. Hopkins Marine Station (HMS) is located at the southern end of the Monterey Bay and is characterized by an irregular rocky coastline (Figure 1a). Two experiments were conducted: 1) experiment A was from 7 March until 4 April of 2018 (yearday 68–94) and 2) experiment B was from 12 October until 1 November of 2018 (yearday 285–305). The experiments, while six months apart, experienced similar offshore wave conditions (H_{rms}) ranging from 0.2 to 1.25 m (not shown). For both experiments the wave direction (θ) was predominantly out of the northwest and peak wave period (T) ranged from 5–12 s. Tides in the Monterey Bay are mixed, mainly semi-diurnal, where the low-low tide always follows the high-high tide with a tidal range of approximately 2 m (Broenkow and Breaker 2005).

A 2015 bathymetric survey was provided by the Sea Floor Mapping Laboratory (SFML) at California State University at Monterey Bay (CSUMB). The SFML survey used a Reson Seabat 7125 multibeam echosounder with a horizontal resolution of 1 meter and a vertical resolution of 0.20 m capturing the large scale bathymetry of the experiment site (Figure 1b). The bathymetry offshore of the experiment site, (Figure 1b) is smooth in the alongshore direction (y) with no abrupt changes in elevation (z), where z=0 at mean sea level (MSL). In the cross-shore direction (x) approaching the rocky reef, elevation increases as expected and again demonstrates consistent smooth transitions, which is indicative of a flat bottom composed of coarse sand (Eittreim et al. 2002). Conversely, within the experiment site (insert Figure 1b) there are abrupt and significant elevation changes in y- as well as in the x-direction. For x= 200–175m, the changes in elevation in x and y are subtle compared to the rest of the site indicating a transition from a sandy and crushed shell bottom to the Edge Of the Rocky reef (referred to as EOR). Approaching the rocky coastline (x=175-50 m) there is large variability in z, which indicates large rock features.

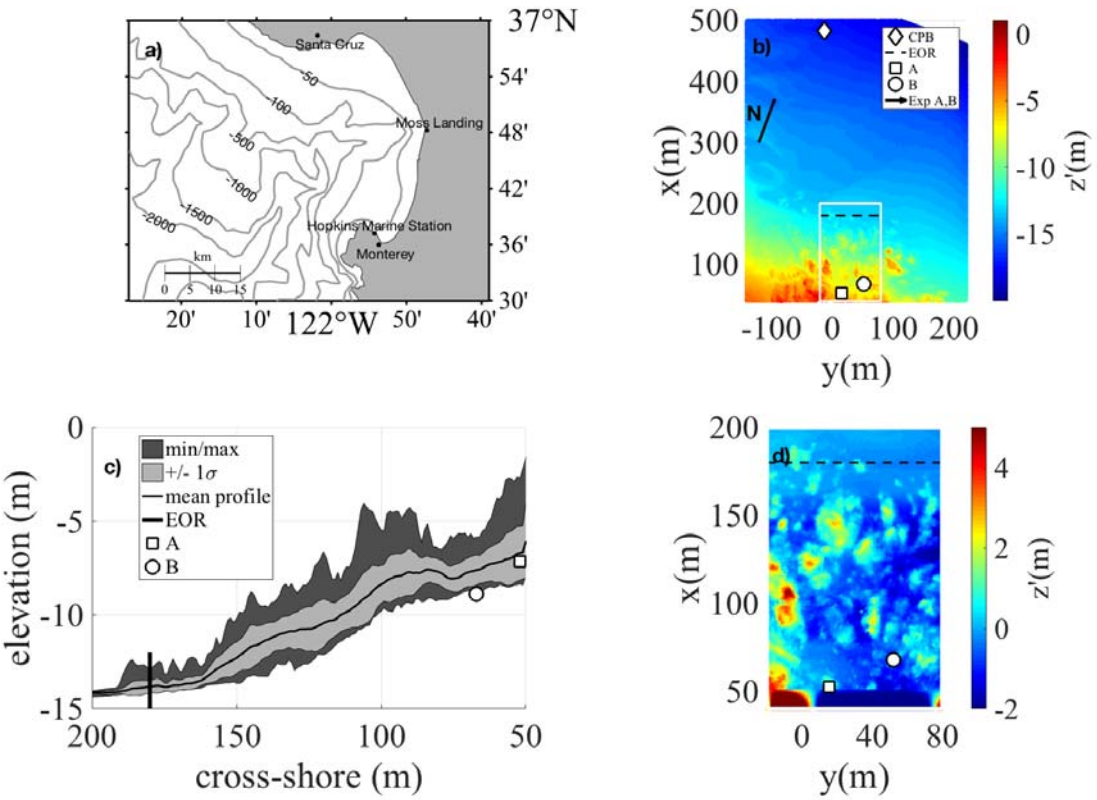

Figure 1. Map of Monterey Bay and its corresponding bathymetry. a) Map of the Monterey Bay identifying the location of HMS, where the grey line is bathymetry contours. b) Bathymetry and instrument layout for experiments A and B. Insert represents the location of experiments A and B. The Edge of the Reef (EOR) is identified by the black dashed line. White circle and square represent instrument locations. x is the cross-shore direction and y is the alongshore direction. c) Cross-shore elevation profile of the experiment site. Thin black line represents the mean bathymetric profile. Dark grey area represents the maximum and minimum elevations from the mean. Light grey area represents +/- 1 standard deviations from the mean. Black vertical line denotes the EOR, while white circle and square represent cross-shore positions and elevations of the instruments. d) The vertical roughness of the experiment area relative to the mean profile.

Cross-shore bathymetric profiles were measured every meter across the experiment site and averaged to create a mean bathymetric profile (Figure 1c). The standard deviation of the mean profile as well as the maximum and minimum elevations from the experiment site are provided in Figure 1c with corresponding instrument locations summarizing the bottom variability. Based on the mean profile of the experiment site (Figure 1c), the mean slope prior to the EOR is mild at 1/65 and shows very little variation. From the EOR (black vertical line) to the end of the experiment site, the mean slope increases and is steeper at 1/17. The variability in the mean profile (black line) are indicative of the undulations due to the Miocene age, igneous rocks that are common on the Central California coast (Eittreim et al. 2002). The block structure of the igneous rocks present often is used to determine their roughness. The standard deviation of the mean profile is approximately 1 m is along the profile. The bathymetry of the rocky reef is complex with large rock features throughout the field site.

Inshore wave estimates were obtained using bottom-mounted RBR Solo-D pressure sensors located well outside of wave breaking in 7.1 m (A) and 8.8 m (B) water depth (Figure 1B). Offshore wave estimates were obtained 430 m to the northwest of the experiment sites in 17.8 m of water (Figure 1b) from the National Data Buoy Center waverider buoy, station 46240 at Cabrillo Point (referred to as Cabrillo Point Buoy, CPB), which is hosted by the by the Coastal Data Information Program at the University of California at San Diego.

Wave energy reflection (R^2) was measured using Acoustic Doppler Current Profilers (ADCPs) deployed during these experiments in shallow-water and outside of these experiments in deeper water using both phased-locked and non-phased-locked methods as described by Huntley and Davidson (1998). R^2 is typically 0.1 for sea and swell waves on this particular rocky reef (Dorantes et al. 2019, in preparation). R^2 is consistent with other R^2 estimates on rough bottoms [10% at Palmyra atoll (Monismith et al. 2015) and 16% at Red Sea coral reef (Lentz et al. 2016)]. It is also consistent with field measures of R^2 (0.09 for 0.1Hz wave frequencies) from a nearby breakwater at Monterey Harbor (Dickson et al. 1995). Monismith et al. (2015) and Lentz et al. (2016) considered R^2 negligible for computing wave energy dissipation, as is assumed here.

B. 3 METHODS

1. Wave Estimates from Pressure

Sea surface elevation spectra ($\eta(f)^2$) were calculated by converting measured dynamic pressure spectra ($p_d(f)^2$, in decibars) using the linear wave theory transfer function at the seabed:

$$\eta(f)^2 = p_d(f)^2 \cosh(kh)^2, \quad (5)$$

where f is wave frequency, k is radian wavenumber, and h is water depth. Spectra were computed for hourly segments using 6 Hanning windows per segment with 50% overlap resulting in 32 degrees of freedom. The root-mean-square (rms) wave height, $H_{rms} = \sqrt{8\sigma^2}$, where σ^2 is the variance of the swell-sea band obtained by integrating $\eta(f)^2$ over f=0.05-0.20 Hz.

Offshore $H_{rms,CPB}$, θ, and T were calculated from directional wave spectra measured by CPB. $H_{rms,CPB}$ are significantly correlated at 95% with values at A and B (r=0.93 and r=0.95) stating the wave measurements at locations A and B are representative of the waves at CPB.

2. Wave Estimates at the Edge of Reef (EOR)

Direct H_{rms} measurements at the EOR are not available for either experiment as sensors were not deployed here. The sea floor is relatively smooth between CPB and the EOR (Figure 1B). $H_{rms,\,EOR}$ were computed by shoaling the $H_{rms,CPB}$ (TG83) to EOR. The shoaled waves from CPB to EOR resulted in less than a 1% difference in H_{rms} between the two positions for experiment A and B. Owing to the minor difference, H_{rms} and T acquired at CPB are used as proxy measurements at EOR.

3. Dissipation

Dissipation seaward of the surf zone, outside of wave breaking, is determined by applying (1) to (3). Assuming the swell waves are described by a narrow-band wave spectrum such that individual waves can all be described as having the same mean wave period, wave heights are well-described by the Rayleigh distribution (TG83). Applying linear wave theory to describe wave velocities at the bed, time averaged energy dissipation by friction for a single wave is described by:

$$\varepsilon_f = \rho f_e \frac{1}{6\sqrt{\pi}} \left(\frac{2\pi f}{\sinh kh} \right)^3 H^3 \, . \tag{6}$$

The average dissipation for all waves is:

$$\overline{\varepsilon_f} = \rho f_e \frac{1}{6\sqrt{\pi}} \left(\frac{2\pi f}{\sinh kh} \right)^3 \int_0^\infty H^3 \, p(H) dH, \tag{7}$$

$$\overline{\varepsilon_f} = \rho f_e \frac{1}{16\sqrt{\pi}} \left[\frac{2\pi f H_{rms}}{\sinh kh} \right]^3, \tag{8}$$

where the Rayleigh probability distribution, p(H), describe the random wave field (TG83). The total amount of dissipation between two locations is given by:

$$\langle \varepsilon_f \rangle = \int_{x_1}^{x_2} \overline{\varepsilon_f} \, dx = \int_{x_1}^{x_2} \frac{dF}{dx} dx = F_2 - F_1, \tag{9}$$

where brackets indicate spatial and temporal averaging. Since $\overline{\varepsilon_f}$ in (8) is a function of H_{rms} and k, which are functions of the local h, the integral of $\overline{\varepsilon_f}$ in (9) cannot be solved directly. Therefore, (9) is solved numerically with an iterative forward-differencing scheme over the measured bathymetric profile. The solution starts with the measured initial condition $F_{1,EOR}$ specified, and (9) solved by varying f_e to match $F_{2,A \text{ or } B}$. The numerically estimated f_e corresponds to a bulk average for the varying rough profile.

C. RESULTS OF DISSIPATION DUE TO BOTTOM FRICTION

F and subsequent $\langle \varepsilon_f \rangle$ were calculated for both experiments between the EOR and A and B respectively (Figure 2). The average reduction in F was 28% between EOR and A and 36% between EOR and B. These reductions are substantial considering the distances between EOR and A and B is only 131 and 116 m apart (Figure 1c). For 18% and 3% of the time during experiment A and B respectively, there were periods when $F_2 > F_1$. This results in $-\langle \varepsilon_f \rangle$, which physically translates to amplification instead of dissipation. There is no clear physical explanation as to why this occurred, as there was no correlation with H_{rms}, T or θ. Therefore, for the results reported here, the data when $F_2 > F_1$ resulting in $-\langle \varepsilon_f \rangle$, are ignored and result in gaps in $\langle \varepsilon_f \rangle$ (Figure 2c,d). The f_e values range from 0.04 to 40.2 with a mean of 8.3 for experiment A (Figure 3c) and 0.03 to 43.8 with a mean of 12.9 for experiment B (Figure 3d). An inverse relationship of H_{rms} to f_e is apparent in both experiments where the largest (smallest) values of f_e occur during the smallest (largest) H_{rms} conditions (Figure 3).

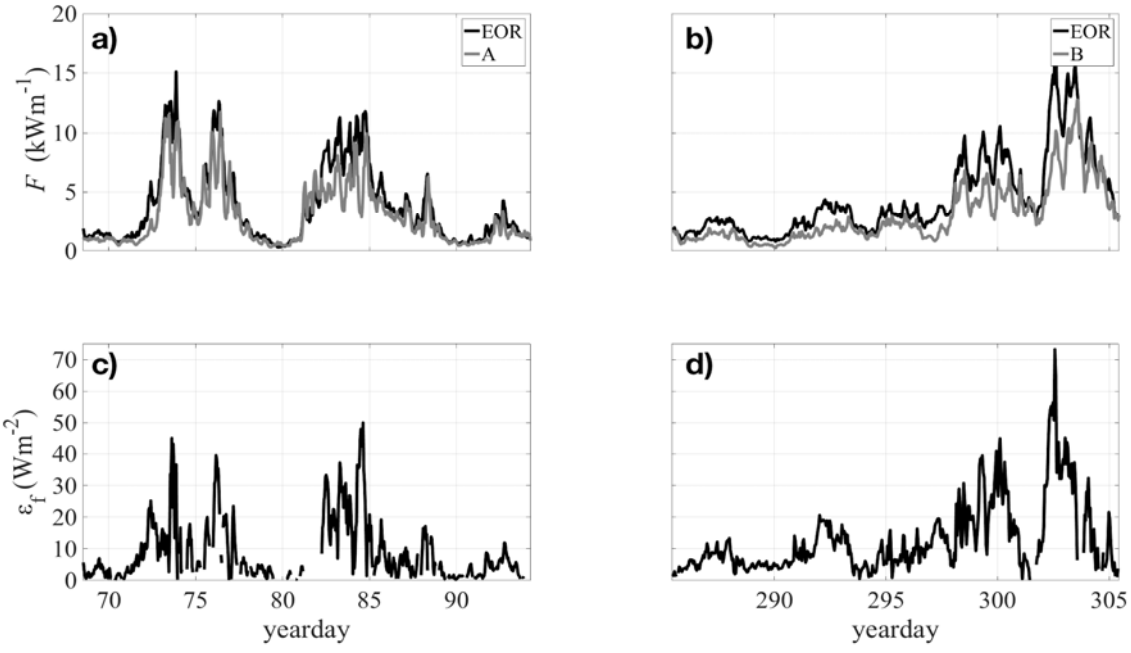

Figure 2. a and b) Time series of wave energy flux at the EOR (black line) compared to A and B (grey line) for experiment A and B; c and d) Time series of wave energy dissipation between EOR and A and B.

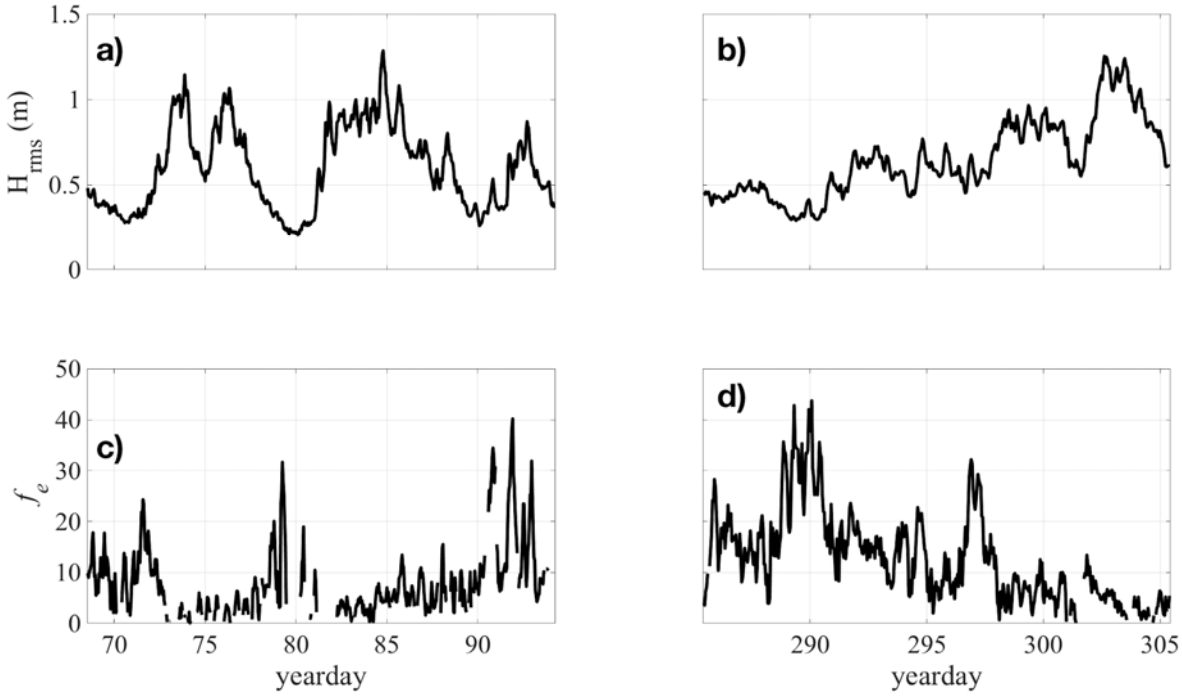

Figure 3. Time series of average H_{rms} between EOR and experiment A (a) and B (b); times series of f_e calculated from (7) for experiment A (c) and experiment B (d).

Lentz et al. (2015) found f_e was related to the water-particle excursion amplitude at the bed, A_b, which for linear wave theory (Dean and Dalrymple, 1984) is given by:

$$A_b = \frac{1}{2}\frac{H_{rms}}{sinh(kh)}. \quad (10)$$

f_e is compared with A_b calculated at the midpoint between EOR and A and B (Figure 4). f_e decreases with increasing A_b. Bin-averaged f_e values ranged from 31.6 for the smallest A_b (smallest wave or shortest period waves or both), to 2.1 for the largest A_b (largest wave or longest period wave or both) (Figure 4 solid black circles).

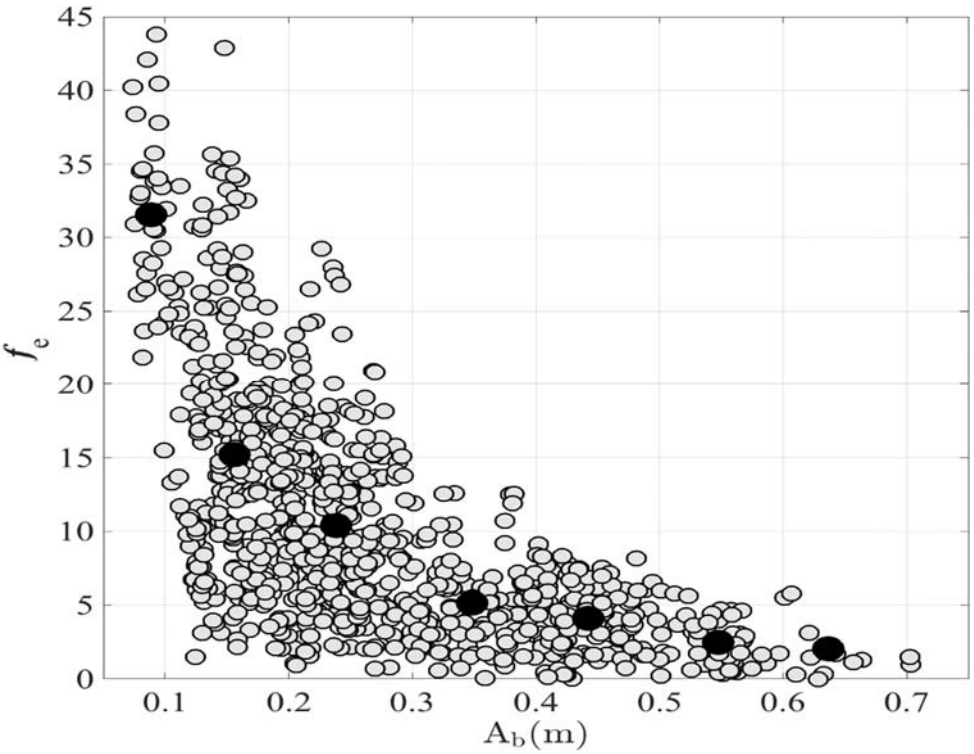

Figure 4. f_e as a function of mean A_b between the EOR and including data from experiment A and B. Grey circles represent individual hourly estimates of f_e. Large black circles are bin-averaged values of f_e.

D. DISCUSSION

1. Bottom Roughness

f_e has been shown to be a function of bottom roughness (Lowe et al. 2005; Monismith et al. 2015; Rogers et al. 2016; Lentz et al. 2016; Yu et al. 2018). Lentz et al. (2016) for coral reefs reported a bottom roughness of 0.1 to 0.4 m with a standard deviation of 0.13 m, which are 7 times smaller than the rocky reef described herein. The resulting 28 and 36% reduction in F from the EOR to A or B as indicated by $\langle \varepsilon_f \rangle$ on the rocky reef cannot be neglected, similar to coral reefs (Lowe et al. 2005; Monismith et al. 2015; Rogers et al. 2016., Lentz et al. 2016). A contributing factor to significant $\langle \varepsilon_f \rangle$ is large bottom roughness resulting in large f_e.

A histogram of the vertical variations (z') about the mean bottom profile is calculated to better understand the bottom roughness (Figure 5). z' ranges +4 to -3 m with

a standard deviation of 0.9 m stating that 87% of the undulations are nearly +/- 1 m from the mean profile. The remaining 13% of the vertical variation is distributed in the larger more extreme undulations of up to +4 m and -3 m highlighting the roughness and spatial variability of the bathymetry. The measured roughness values are the largest seen to date from field effort.

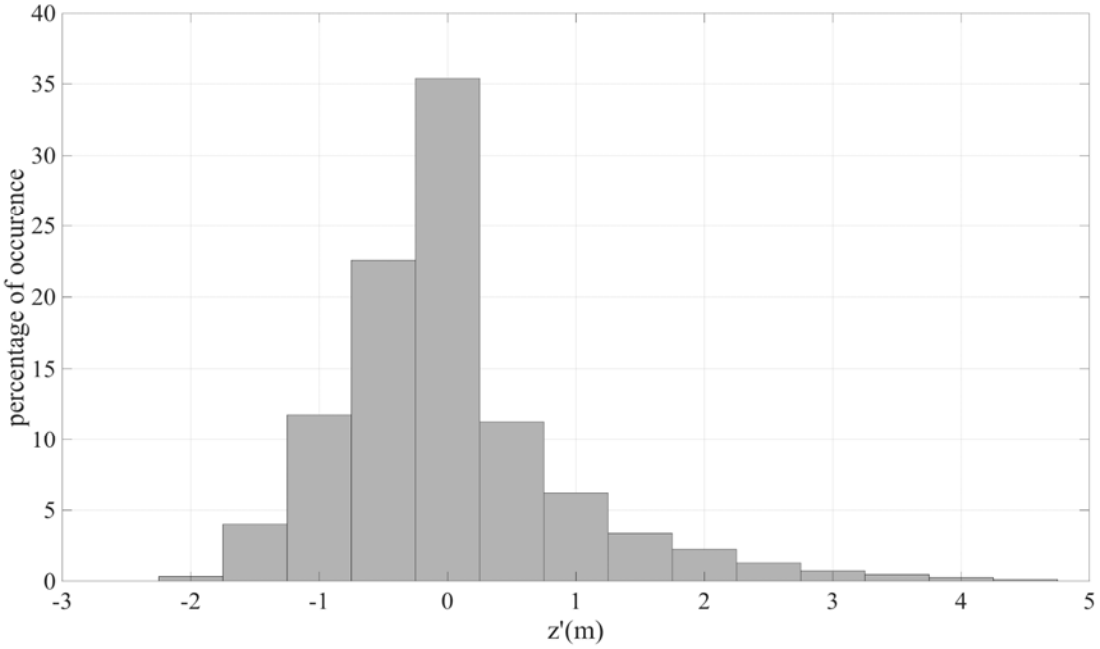

Figure 5. Histogram of detrended vertical elevations (z') from Figure 1d.

A two-dimensional (2D) autocorrelation was performed on z' (Figure 1d) to examine the ensemble-averaged horizontal spatial scales and symmetry of roughness elements (Figure 6). x- and y-scales are determined by the e-folding decorrelation. In the x- and y-direction, there is an apparent primary undulation scale of approximately 14 m and 8 m (Figure 6). A slight asymmetry in the x-direction exists. On average, the bottom is composed of large rock features that are approximately 14 m long, 8 m wide and can range in extrema height of up to 7 m. It should be of no surprise that the large ε_f leads to a larger range of f_e for a rocky reef than previously determined for rough coral reefs.

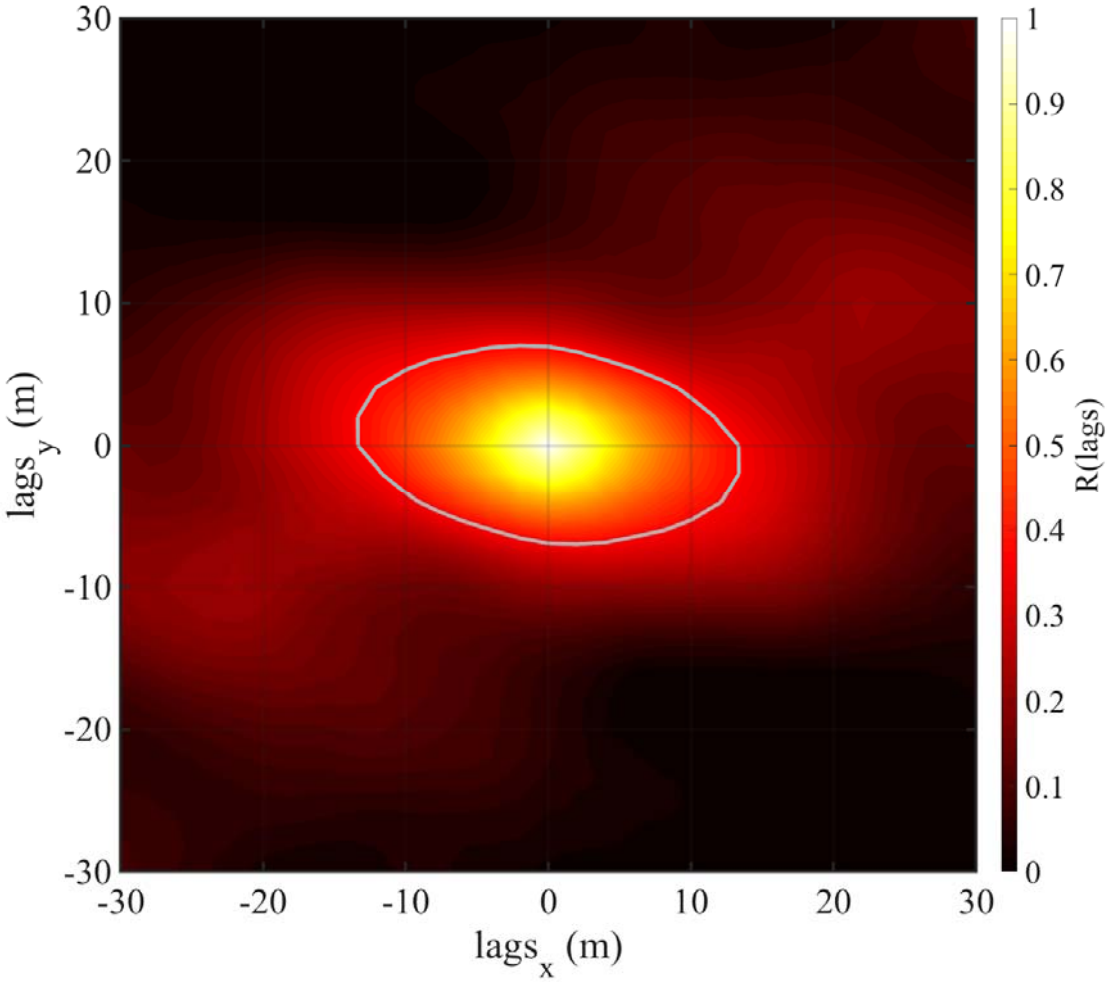

Figure 6. 2D autocorrelation of the detrended bathymetry. Grey circle identifies the e-folding scale.

2. Midpoint Method for Energy Friction Factors

Owing to a lack of detailed bathymetric profiles, Monismith et al. (2013), Monismith et al. (2015), Rogers et al. (2016), and Lentz et al. (2016) solved (8) by calculating $\langle \varepsilon_f \rangle$ at the midpoint between the two measured locations and then solved for an average f_e (referred to as $f_{e,midpoint}$). To examine the error associated with using the "midpoint" method, $f_{e,midpoint}$ is compared with f_e (Figure 7). Although, the root-mean-square error between f_e and $f_{e,midpoint}$ is 4.5, there is scatter and obvious biases. f_e is proportional to f^3 (f is wave frequency) indicating a sensitivity to wave period (as shown in Figure 7).

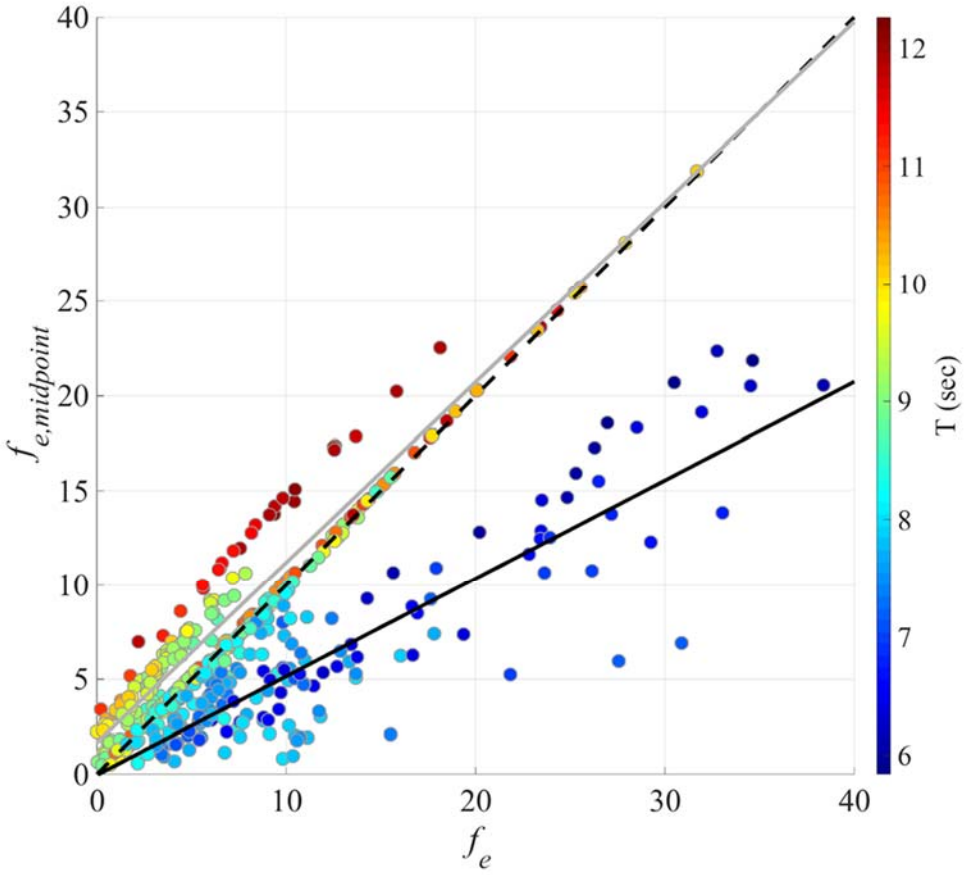

Figure 7. Scatter plot of $f_{e,midpoint}$ compared to f_e where the dot color represents T, which is color scaled to the right. The dashed line is a 1:1 line. The grey line is the linear fit for long period waves. The black line is the linear fit for short period waves.

For short period waves (T<9s), $f_{e,midpoint}$ is underestimated by a factor of 2. Conversely, there are clear biases for T >11 s, where the use of midpoint averages over predicts by 25%. Analyzing other parameters such as wave steepness (H_{rms}/L), tide, A_b, θ, and H_{rms}, provided no clear indication as to why the biases exist. One plausible explanation for the biases is $\langle \varepsilon_f \rangle$ is proportional to H_{rms}^3, f^3, and $\sinh(kh)^3$ (8). In the integration of (8), two competing factors determine the value of ε_f. As waves approach shallow water, $\sinh(kh)$ approaches kh such that $\left(\frac{2\pi f}{kh}\right)^3$ approaches $g^{\frac{3}{2}}h^{\frac{-3}{2}}$. As the waves shoal, ε_f increases as a function of $h^{-3/2,}$ competing with decreases in H_{rms}^3. Using the midpoint to calculate $\langle \varepsilon_f \rangle$ assumes a linear increase in $\langle \varepsilon_f \rangle$ and disregards the proportionalities stated

above. Assuming a linear increase in $\langle \varepsilon_f \rangle$ leads to an underestimate of the measured dissipation between the two stations requiring f_e to compensate resulting in larger values of f_e and a potential bias high (Figure 7). Due to the bias of the results based on averages, numerically solving for f_e across the profile is the preferred method and was applied to this analysis.

3. Relating f_e to σ_b

f_e is related to hydraulic roughness (z_o) and A_b through several empirical relationships based on laboratory results (e.g., Grant and Madsen, 1982; Nielsen, 1992; Soulsby, 1997). Soulsby (1997) finds:

$$f_e = 1.39\left(\frac{A_b}{z_o}\right)^{-0.52}. \quad (11)$$

It is not possible to directly measure z_o, consequently estimates of z_o result from other empirical models. This adds an additional layer of uncertainty. $z_o = \frac{k_n}{\beta}$, where k_n is the geometric bottom roughness scale. Henceforth, σ_b represents k_n. β is a proportionality coefficient that relates k_n to z_o based on the environment whose roughness is being quantified (Bangold 1941). β have been reported anywhere between 2.5 and 100 for engineering and atmospheric boundary layers depending on the given environmental conditions (Raupach et al. 1991; Britter and Hanna 2003; Jimenez 2004; Nield et al. 2013). Owing to the large range of β creating uncertainty in z_o, f_e are computed directly with measured σ_b, which states β is one. By relating f_e to A_b as a function of σ_b every parameter is based on an actual measurement instead of a fit to an empirical relationship. Following Yu et al. (2018) and applying the Buckingham Pi theorem, $\frac{A_b}{\sigma_b}$ was chosen as a dimensionless parameter to relate to f_e (Figure 8).

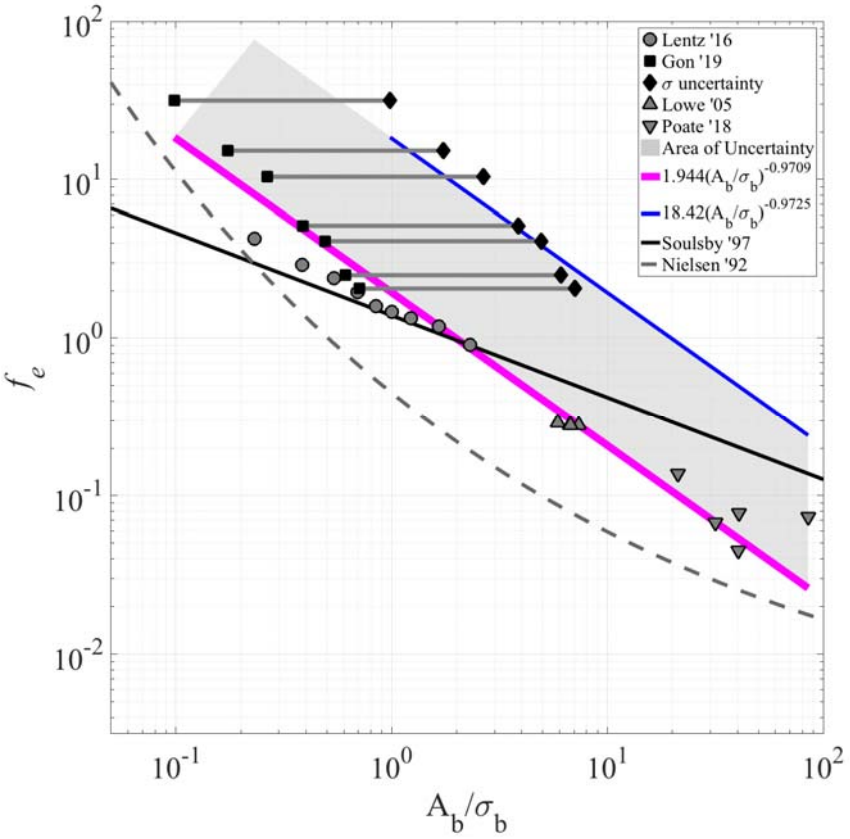

Figure 8. Bin-averaged f_e (symbols) plotted as a function of A_b/σ_b, from multiple field experiments. Horizontal bold grey lines represent uncertainty for smaller scales of bottom roughness. Solid black line represents Soulsby (1997) relationship, grey dashed dot line represents Nielsen (1992), magenta line represents a best fit relationship based on all data considered with a σ_b=0.9 the solid blue line represents a best fit based on all data considered with a σ_b=0.09. Grey area is the area of uncertainty that exists based on a range of bottom roughness.

Three additional datasets are used to establish a relationship between f_e and σ_b covering four orders of magnitude: Red Sea coral reef (Lentz et al. 2016), the reef at Kaneohe Bay (Lowe et al. 2005), five different rock platforms with varying morphological features (Poate et al. 2018). Datasets were only included if supporting physical measures of roughness were available. For each dataset, bottom roughness is defined as $1\sigma_b$. The largest σ_b of 0.9 m is the rocky reefs, while the Red Sea and Hawaiian reef were 0.13 m and 0.04 m respectively. In all three of these cases, bin averaged values for each experiment are representative of the changing wave conditions throughout each experiment. The

results from Poate et al. (2018) are individual values of σ_b, a mean A_b and corresponding mean f_e from five Type A rocky platforms where σ_b range from 0.02 m to 0.04 m. Soulsby's 1997 empirical relationship (11) is plotted in Figure 8 as a solid black line. Data from the Red Sea coral reef are in good agreement and generally follow the Soulsby relationship as Lentz et al. (2016) noted, but it does not appear to fit the other data sets. Based on the results from all of the field data presented, a power-law empirical relationship was established which relates values of f_e based on A_b and σ_b:

$$f_e = 1.944\left(\frac{A_b}{\sigma_b}\right)^{-0.9709} \tag{12}$$

The advantage of (12) is direct estimates of f_e can be determined based on wave measurements and σ_b. The large σ_b and concomitantly large f_e extend laboratory experiments (Myrhug et al. 2001; Soulsby et al. 1993; Mirfenderesk and Young 2003). As noted by Lentz et al. (2016) and Rogers et al. (2016), f_e at Palmyra Atoll, the Red Sea Reef and now the rocky reef, are an order of magnitude larger (Nelson 1996; Lowe et al. 2005).

Yu et al. (2018) computed large eddy simulations of turbulent boundary layers forced by waves over a rough bottom composed of evenly spaced hemispheres. They considered cases where A_b were similar to the roughness elements described by the diameter, D, of the hemispheres. f_e values are parameterized on $\frac{A_b}{D}$. Of note by using D, the vertical length scale is the sole parameterization for roughness and does not change regardless of hemisphere spacing. Conversely, if the roughness is described by σ_b, both the hemisphere spacing as well as the vertical height of the hemispheres is included in the parameterization. As the hemisphere spacing increases, σ_b will decrease for a given x, resulting in larger $\frac{A_b}{\sigma_b}$ which would fit closer to Nielsen's empirical curve (dashed line in Figure 8).

Yu et al. (2018) are able to separate the bottom stress into inertial and form drag forces. Inertial forces are due to the mass of the fluid having to be accelerated around the rocks (hemispheres). The larger the rock, the more acceleration required and the larger the inertial forces. Owing to the presence of the shear stress at the bed, there is work done by wave velocities against the shear stress. The inertial forces being a function of the

acceleration are in quadrature with the velocity of the fluid, and therefore do not contribute to the work done by the waves (Yu et al. 2018). Therefore, inertial forces do not contribute to bottom friction wave dissipation. Therefore, f_e is solely a function of form drag. When $A_b > \sigma_b$, the curvature of the hemispheres (roughness) is relatively small resulting in flow separation with large form drag and small inertial forces. In this case, f_e is equal to the total wave friction factor (f_w) owing to the negligible contribution from the inertial forces. Conversely, when $A_b \leq \sigma_b$, the curvature of the hemispheres is large resulting in little flow separation and small form drag with dominant inertial forces and can be classified as smooth flow conditions (Yu et al. 2018). In these cases, $f_e < f_w$, a paradox arises as the rocky reefs presented here and the Red Sea coral reef presented by Lentz et al. (2016) have the largest measured values of roughness and are in the regime dominated by inertial forces as identified by Yu et al. (2018), but report the largest field measurements of f_e to date. The question that remains is why is f_e so large if the dominant force is inertial? The rocky reef is composed of large rock features with average cross-shore and alongshore widths of 14 m and 8 m and heights of up to 1 m could create smooth flow as identified by Yu et al. (2018). What is not accounted for is all of the small-scale features, which exist on top of these large-scale features. Upon closer visual inspection via swimmers there are multiple scales of roughness, which are not accounted for in the estimated roughness. The rock structures are not smooth, they are jagged and have peaks and valleys and different crevices. Additionally, the ecosystem is diverse and made up of different rocky intertidal invertebrates and algae which are on centimeter and smaller scales and all fixed to the larger rock structures.

It is hypothesized that the large values of f_e and resulting dissipation by friction are owing to multiscale biological roughness and that the smaller features hosted by these large rocks are responsible for creating flow separation due to form drag, which would explain the large amount of dissipation and resulting large f_e. In Figure 8, a range of values for σ_b spanning an order of magnitude (0.09-0.9 m) are applied to represent varying bottom roughness. The black line connecting the measured value of σ_b (0.9 m) to a hypothesized value of intertidal organisms on the rocks σ_b (0.09 m) represents the uncertainty in σ_b. Of note, the bathymetry of Lentz et al. (2016) also did not have the fine scale resolution to

resolve the smaller scales. In the calculation of possible solutions for smaller scale σ_b, the Lentz et al. (2016) data are not permutated and are omitted for this follow-on analysis. By differentiating the roughness scale, a scenario can be created where form drag would actually dominate allowing for flow separation and larger values of f_e. Higher resolution surveys are required to be able to consider the effects of the smaller rocky features as well as the marine biota present. A second empirical relationship is solved for using the same datasets less Lentz et al. (2016):

$$f_e = 18.42\left(\frac{A_b}{\sigma_b}\right)^{-0.9725}. \quad (13)$$

By applying σ_b that is representative of the smaller scales present on the rocks, the curve steepens and a large area of uncertainty, represented by the filled in grey area in Figure 8 is established. The area of uncertainty represents possible f_e based on varying σ_b. Accounting for the large-scale and the small-scale bathymetric changes is an area that needs further exploration.

THIS PAGE INTENTIONALLY LEFT BLANK

III. NEARSHORE WAVE TRANSFORMATION OVER A ROCKY REEF SHORELINE

Shallow water wave transformation, inside of wave breaking, over a rocky reef shoreline at HMS in Monterey Bay, California, is studied. The rocky reef bottom roughness measured offshore in water depths between 17 and 5 m at HMS is 8–10 times rougher than coral reefs (see Chapter I). An array of pressure sensors was deployed to measure waves for evaluating the relative dissipation due to bottom friction and wave breaking. Similar to Lentz et al. (2016), H_{rms} is observed to be a nonlinear function of h, differing from (4). An analytical model for shallow-water wave transformation on a plane sloping bottom with bottom friction is derived to compare with observations. The sensitivity of the non-linear relationship is evaluated with the analytical model for varying wave heights, bottom slopes, and friction factors. The observations are used to obtain the breaking wave parameter and the energy friction coefficient. With these parameters, the TG83 wave transformation model, which includes dissipation by bottom friction and wave breaking, is evaluated across the measurement array.

A. FIELD EXPERIMENT

Surface gravity waves were observed during two monthly deployments composed of an array of bottom-mounted pressure sensors positioned across the rocky reef and intertidal zone at two different sites off of HMS. HMS is located at the southern end of the Monterey Bay, California, and is characterized by an irregular rocky coastline (see Figure 9). Each deployment, while six months apart, experienced similar offshore H_{rms} (0.2–1.25 m). Wave direction was predominantly out of the northwest and peak wave period, T, ranged from 5–12 s. The tides are mixed, mainly semi-diurnal, with a tidal range of approximately 2 m (Broenkow and Breaker 2005).

Figure 9. Picture from Stanford Hopkins Marine Station at low tide showing the irregularities of the rocky coastline.

The exposed rock structures seen in Figure 9 represent a complex network of channels that is also representative of the bathymetry of this site. A 2015 bathymetric survey that extends to a shallow water depth of 5 m was provided by the CSUMB. The SFML used a Reson Seabat 7125 multibeam echosounder with a horizontal resolution of 1 m and a vertical resolution of 0.20 m in the survey. A kayak outfitted with a system was used to augment the SFML survey. In addition, walking surveys were performed on the reef flat using a survey-grade GPS mounted on a backpack on a human (Figure 10).

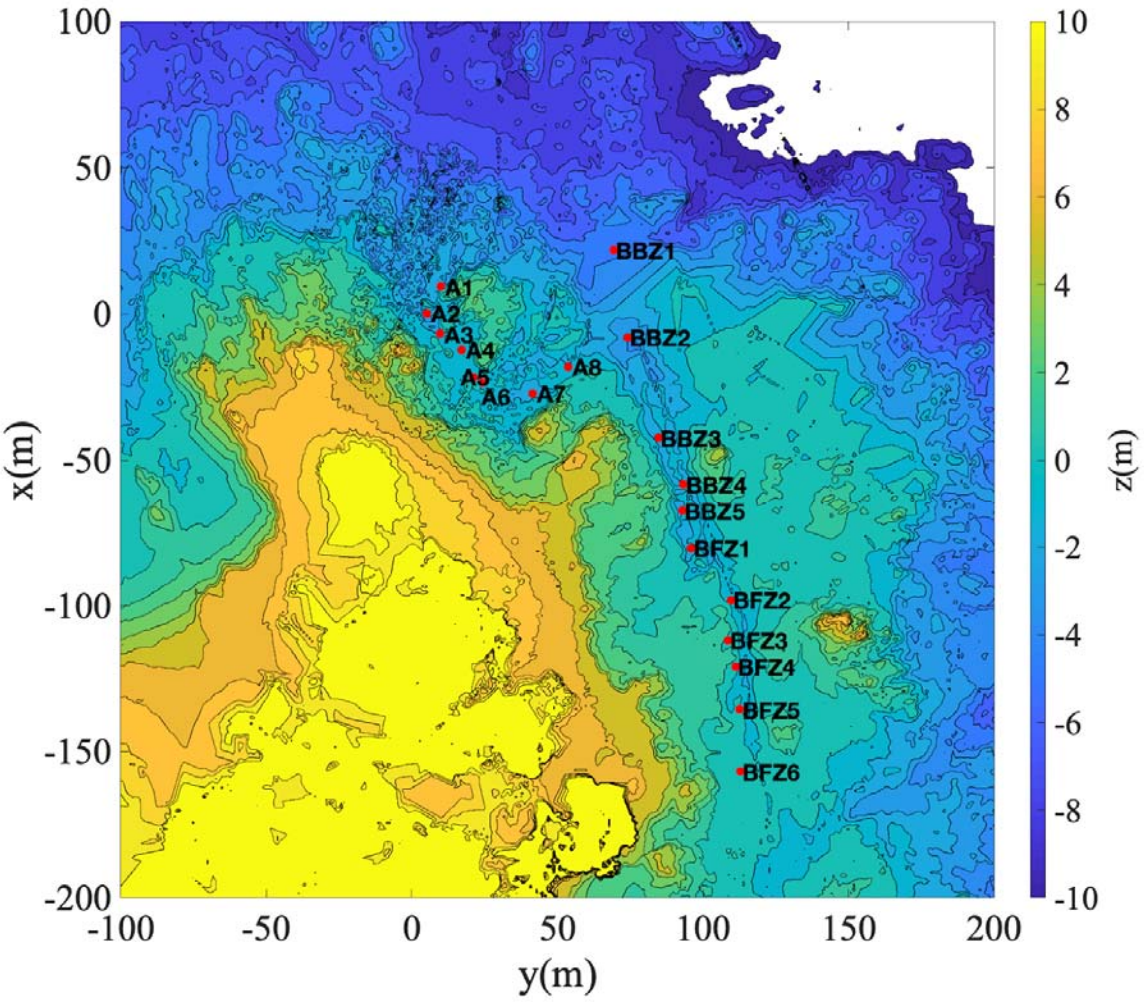

Figure 10. Bathymetry and topography of HMS contoured in 1 m increments. Red dots represent instrument locations for site A and B.

The first experiment occurred at site A during March 2018. A total of 8 pressure sensors sampling at 2Hz were deployed in a spatial array around a subaerial rocky outcrop (Figure 10). Site A is not a well-defined channel, allowing incoming waves to enter from different directions at either A1 or A8 (Figure 10) and converging on the shallowest point at A5 (Figure 11a). Of note, A1 was located at the edge of a shallow water reef, on a submerged rock, where wave breaking was observed visually. Owing to the subaerial rocky outcrop and channel complexity that allows waves to enter from two locations, analysis of wave energy fluxes between stations was difficult. The data proved valuable and will be discussed throughout. The experience from site A points out the difficulty of conducting

experiments on a new topic without a priori knowledge. Building on the lessons learned from the first experiment, a second experiment was conducted at site B in October 2018 at a nearby location (80 m away). A spatial array of 11 wave sensors sampling at 2 Hz was deployed in the cross-shore allowing for waves to be analyzed in the primary direction of wave propagation. The field site is divided into two zones: 1) a breaking wave dominated zone (BZ) and 2) a bottom friction dominated zone (FZ). For site B, BZ is characterized by a steeper bottom slope 1/30, located in z=-6 to -2 m relative to MSL (Figure 11). For the FZ, the slope is 1/70 with a maximum depth change of 1 m (Figure 11).

Sea surface elevation spectra were calculated hourly by converting pressure spectra measured at each station using the linear wave theory transfer function (Dean and Dalrymple, 1984). The rms wave height, $H_{rms} = \sqrt{8\sigma^2}$, where σ^2 is the variance of the swell-band obtained by summing the sea-surface elevation spectrum over frequencies 0.05-0.20 Hz. Mean cross-shore H_{rms} for the entire experiments at A and B are shown in Figures 11b and 11d.

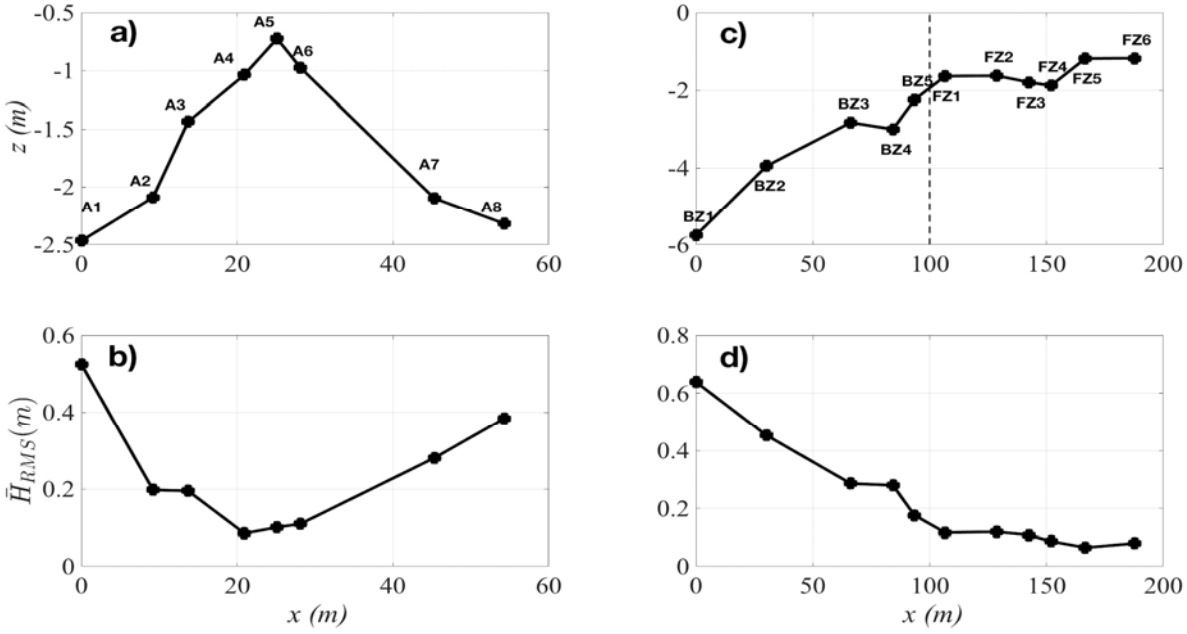

Instrument elevations (black circles) as a function of distance for site A, a), and site B, c). Experimental mean H_{rms} as a function of distance for site A, b), and site B, d). The vertical dashed line in c) denotes the separation of BZ and FZ stations.

Figure 11. Instrument elevations and experimental mean H_{rms}

B. DISSIPATION DUE TO WAVE BREAKING AND FRICTION

Dissipation results in a change in wave energy flux between two stations over a given distance ($\frac{\partial EC_{gx}}{\partial x}$). Assuming a channelized flow, changes in flux are only a function of the cross-shore direction (x). Dissipation occurs from the two primary mechanisms by breaking ($\langle \varepsilon_b \rangle$) and bottom friction ($\langle \varepsilon_f \rangle$):

$$\frac{\partial EC_{gx}}{\partial x} = \langle \varepsilon_b \rangle + \langle \varepsilon_f \rangle, \tag{14}$$

where E is the energy density, C_{gx} is the group velocity in the cross-shore direction, and x is the cross-shore direction (TG83).

Shallow water wave breaking occurs when the waves become unstable as the velocity at the wave crest exceeds the phase velocity of the waves. LeMehaute (1962) first suggested the wave breaking process could be modeled as a bore. Following the Stoker (1957) description for the average rate of energy dissipation per unit area and substituting for the volume discharge of the bore by a breaking wave by Hwang and Divoky (1970) where $Q = \frac{Ch}{L}$, C is the wave speed and L is the wavelength, and when substituted into (15) gives the rate of energy dissipation for each individual bore (Battjes and Janssen, 1978):

$$\varepsilon_b \simeq \frac{f}{4} \rho g \frac{(BH)^3}{h}, \tag{15}$$

where f is the peak frequency of the wave spectrum, ρ is the density of water, g is the gravitational constant, H is the wave height measured as the maximum to the minimum of the bore face, and B is the breaker coefficient O(1), which is a function of the proportion of foam on the face of a breaking wave. The wave heights of a Gaussian distributed surface elevation are well described by a Rayleigh distribution, *P(H),* even during wave breaking (TG83). While the Rayleigh distribution describes the wave field well, only breaking waves contribute to dissipation by breaking. To identify which waves are breaking, a breaking wave height distribution is defined as a subset of the Rayleigh distribution,

$$P_b(H) = W(H)P(H), \tag{16}$$

where W(H) is an empirical weighing function given by

$$W(H) = \left(\frac{H_{rms}}{\gamma h}\right)^n \left[1 - exp\left(-\left(\frac{H}{\gamma h}\right)^2\right)\right] \leq 1 \quad (17)$$

where γ is the breaking parameter and n is a variable to be determined from the observations. The weighting favors larger waves as they have a greater probability of breaking (TG83). As waves shoal and progress into shallow water, the highest waves of the distribution break first, followed by more of the waves until all waves are breaking referred to as saturation. At saturation when all waves are breaking, wave heights can be described as depth-limited by (4). The average rate of energy dissipation by all breaking waves across the distribution is:

$$\langle \varepsilon_b \rangle = \frac{B^3}{4} \rho g \frac{f}{h} \int_0^\infty H^3 P_b(H) dH \quad (18)$$

Substituting (16) and (17) into (18) and integrating, the average energy dissipation due to wave breaking is given by (TG83):

$$\langle \varepsilon_b \rangle = \frac{3\sqrt{\pi}}{16} \rho g B^3 f \frac{H_{rms}^5}{\gamma^2 h^3} \left[1 - \frac{1}{\left(1+\left(\frac{H_{rms}}{\gamma h}\right)^2\right)^{\frac{5}{2}}}\right]. \quad (19)$$

Dissipation due to bed friction (ε_f) is given by:

$$\varepsilon_f = \overline{\tau_b u_b}, \quad (20)$$

the overbar indicates time averaging, u_b is the wave velocity at the bed and τ_b is the bottom shear stress defined by (Jonsson 1966):

$$\tau_b = \frac{f_e}{2} \rho \overline{u_b |u_b|}, \quad (21)$$

where f_e is the energy friction factor. Using linear wave theory to describe wave velocity in (21), the average dissipation over the Rayleigh distribution for all waves due to bed friction is (TG83):

$$\langle \varepsilon_f \rangle = \rho \frac{f_e}{2} \frac{1}{16\sqrt{\pi}} \left[\frac{2\pi f H_{rms}}{sinh\, kh}\right]^3. \quad (22)$$

The f_e is a function of the bottom roughness (σ_b) and the orbital excursion (A_b):

$$A_b = \frac{1}{2} \frac{H_{rms}}{sinh(kh)} \quad (23)$$

where k is the wave number. If σ_b is known, f_e can be solved for using the empirical relationship derived in Chapter II where:

$$f_e = 1.944\left(\frac{A_b}{\sigma_b}\right)^{-0.9709}. \quad (24)$$

The rocky reef at HMS is extremely rough with a measured offshore $\sigma_b$of 0.9 m (Chapter II). From Chapter II, ε_f has been shown to be important outside of wave breaking and is expected to be important throughout the rocky reef.

Wave dissipation owing to bottom friction only, over a plane sloping beach is examined. By restricting the analysis to shallow water, an analytical solution is obtained. Starting with the basic wave transformation equation (14) and energy dissipation by friction formulation (22):

$$\frac{dEC_g}{dx} = \rho\frac{f_e}{2}\frac{1}{16\sqrt{\pi}}\left(\frac{2\pi f H_{rms}}{sinh\ kh}\right)^3. \quad (25)$$

By restricting the analysis to shallow water waves, h/L<1/20, sinh kh goes to kh and

$$C_g = C = \frac{\omega}{k} = \sqrt{gh}. \quad (26)$$

Using the substitutions $y = {H_{rms}}^2 h^{\frac{1}{2}}$ and $h = x\ tan\beta$, (22) can be written as

$$\frac{dy}{dh} = \frac{f_e}{4tan\beta\sqrt{\pi}}\frac{y^{\frac{3}{2}}}{h^{\frac{9}{4}}}. \quad (27)$$

Separating variables and integrating gives:

$$-2y^{\frac{-1}{2}} = -ah^{\frac{-5}{4}} + const, \quad (28)$$

where:

$$a = \frac{f_e}{5tan\beta\sqrt{\pi}}. \quad (29)$$

Assuming initial conditions in shallow water such that:

$$y = y_0 = H_{rms0}^2 h_0^{\frac{1}{2}} \quad at \quad h_0 \leq \frac{L}{20}, \quad (30)$$

solving for the constant and then substituting for y to solve for H_{rms}:

$$H_{rms} = \left(\frac{a}{2}\left(h^{-1} - h^{\frac{1}{4}}h_0^{\frac{-5}{4}}\right) + \frac{h^{\frac{1}{4}}}{H_{rms0}h_0^{\frac{1}{4}}}\right)^{-1} \quad for\ 0 \le h \le h_0. \qquad (31)$$

The analytical solution (31) will be referred to as the Gon, Thornton and MacMahan (GTM) model for wave dissipation due to friction on a plane sloping beach.

C. RESULTS

1. γ in the Breaking Zone and Wave Breaking Due to Friction in the Friction Zone

At sites A and B, all measured H_{rms} as a function of h are plotted for individual stations (Figure 12a, Figure 13a). The $H_{rms}(h)$ vary owing to offshore wave conditions and to variation in h as the 2m tide goes up and down. The stations are located in different mean depths of water relative to MSL ranging from 2.5 to 0.7 m for stations A1-A8 and 5.3 to 1.2 m for all stations at site B (Figure 12a, 13a). In general, $H_{rms}(h)$ decreases with decreasing h per station associated with the tide (Figure 12a, 13a—black horizontal line for tidal range) and across stations. For the deeper (h>2 m) stations (A1, A2, A7, A8, and BZ1-BZ5), there is a larger spread in $H_{rms}(h)$ (black dots in Figure 12a, 13a). For shallower (h<2 m), the spread in $H_{rms}(h)$ is reduced at A4-A6 and FZ1-FZ6 (red dots in Figure 12a, 13a). In addition, for the shallow stations, $H_{rms}(h)$ appears to vary non-linearly with h.

A1 was the only sensor deployed on the outer edge of the rocky reef where wave breaking was visually observed to occur persistently. It is believed that the upper limit $H_{rms}(h)$ for A1 represents the depth-limited wave saturation, γ, for HMS. γ for A1 is estimated by first computing the mean of the top 15% of the waves ($\overline{H_{rms,15}}$) as a function of h bins (plotted as large red circles in Figure 12b). A linear fit was performed on $\overline{H_{rms,15}}$, such that the y-intercept was forced to equal zero. The slope of the line (Figure 12b, red line) represents γ= 0.29 that corresponds to wave saturation. For HMS, $\frac{H_{rms}}{h} \geq 0.29$ is indicative of wave breaking and applied to all estimates.

On the leading edge of A1, A8 and BZ1 a near linear limit exists for $H_{rms}(h)$, which is close to γ= 0.29 suggesting depth-limited breaking is obtained (Figure 12a, 13a magenta dashed line). For all other stations, $H_{rms}(h)$ is much lower than γ= 0.29 (Figure 12a, 13a magenta dashed line) suggesting that other processes are responsible for the local limitations.

For site A, the average $H_{rms}$is reduced by 64% between A1 and A3 over 14 m and 74% between A8 and A6 over 25 m (Figure 3b). At site B, the average H_{rms} was reduced by 55% between BZ1 and BZ3 over 60 m (Figure 11d).

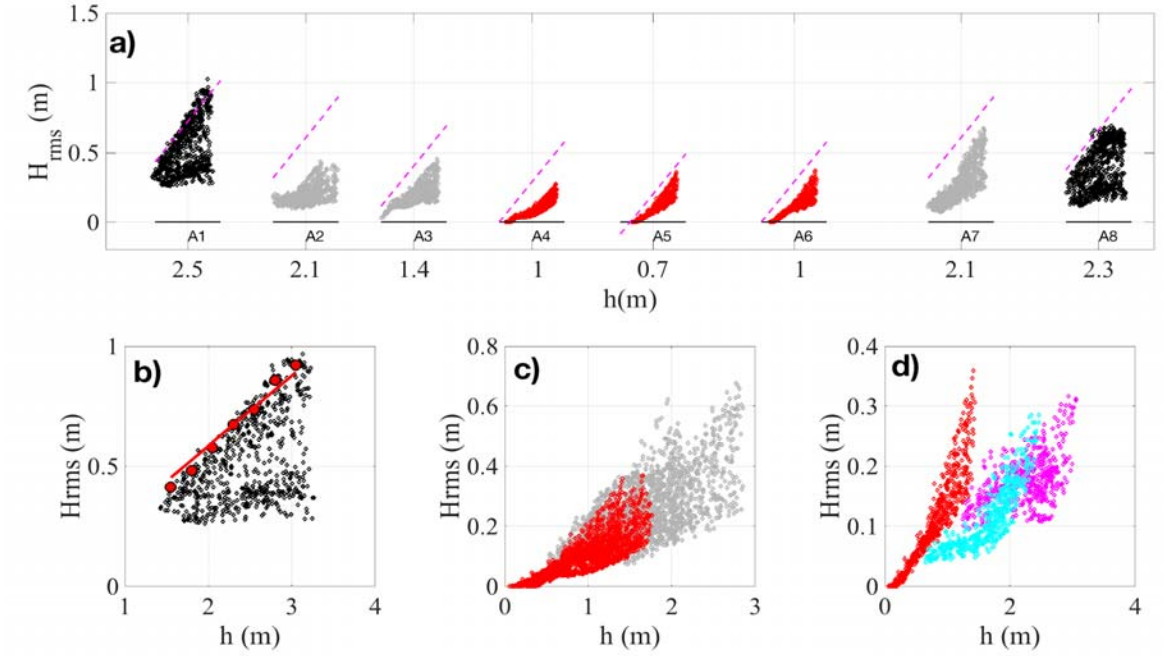

Figure 12. Hrms as a function of h for experiment A. a) $H_{rms}(h)$ for stations A1-A8. Stations have been qualitatively separated based on response described by the dot color. Black dots represent deep stations, grey dots represent transition stations and red dots represent the shallow stations. Horizontal black lines represent +/-1 m tide. Dashed magenta line represents wave saturation $\gamma = 0.29$; b) $H_{rms}(h)$ from A1. Large red circles are $\overline{H_{rms,15}}$. The red line is the linear fit representing $\gamma = 0.29$, where the y-intercept was forced to zero; c) $H_{rms}(h)$ for A2-A7; d) $H_{rms}(h)$ for A5 (red dots), FZ1 (cyan dots), and BZ5 (magenta dots).

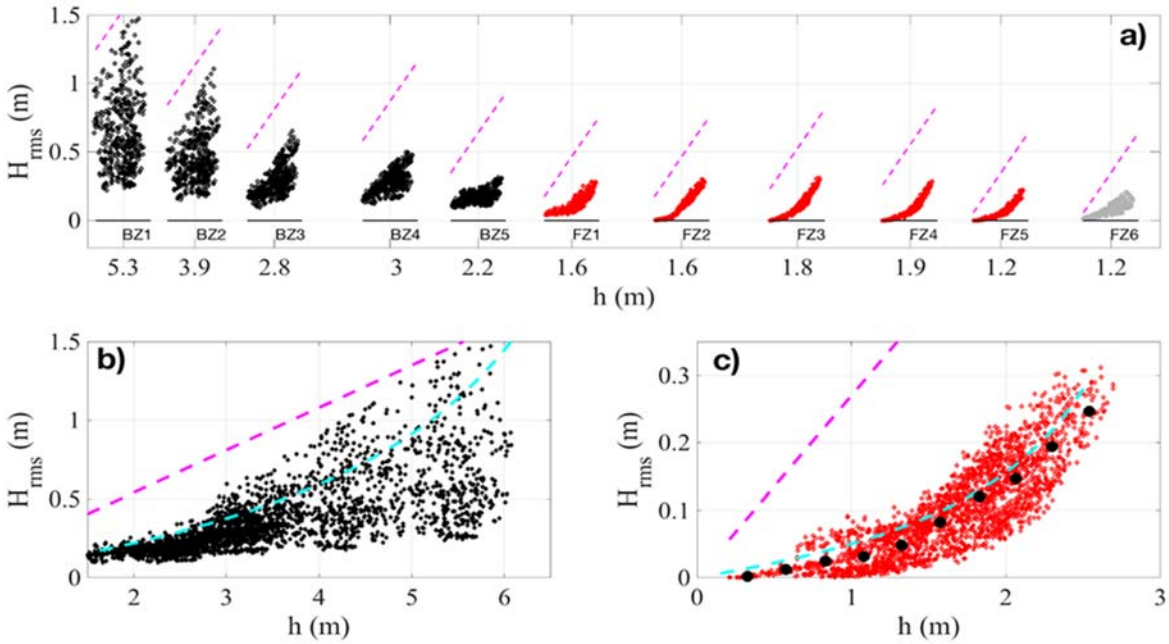

Figure 13. Hrms as a function of h for experiment B. a) H_{rms}(h), where BZ stations are described as black circles, FZ stations are described by red circles, and FZ6 is described by grey circles. Stations are plotted based on their cross-shore location from offshore to onshore. Horizontal black lines represent +/-1 m tide. b) H_{rms}(h) for BZ stations. c) H_{rms}(h) for FZ stations. Black circles are bin-averaged H_{rms}(h). Dashed cyan line in b) and c) represents the GTM analytical solution. Dashed magenta line in all subplots represents wave saturation, $\gamma = 0.29$.

In summary, there is a rapid reduction in H_{rms} across the reef (Figure 11b,d). Variations in $H_{rms}(h)$ are found to be much lower than γ= 0.29, particularly for stations located in shallower water depths (h<2 m) (Figure 12a, 13a). $H_{rms}(h)$ collapses to a non-linear fit for shallower water stations. These results suggest that bottom friction by the rough rocky reef bottom is the dominant dissipation process in wave transformation that differs from sandy beaches.

2. Energy Coefficients, f_e

The dissipation by bottom friction (22) is parameterized by f_e, which is solved for as the residual of the analysis. The measured change in energy flux, F, between adjacent pairs of stations is used as input to (14), with the dissipation by breaking specified by (19) and bottom friction specified by (22) at the forward station where f_e is solved. In Chapter II, large f_e were found offshore and attributed this large bottom roughness offshore. In the BZ and in the FZ, bin-averaged f_e, ranged 3.8 to 8.2 and were inversely proportional to A_b which is consistent with Chapter II (Figure 14). A_b from (23) is a function of H_{rms}, h, and T. In shallow water,

$$A_b \sim H_{rms} T h^{-1/2} \tag{32}$$

The larger f_e values for small A_b is partially due to the greater number of excursions to dissipate energy for shorter wave periods. For a particular case of waves transforming cross-shore, T is assumed constant, but H_{rms} and h vary. As H_{rms} and h change in the BZ and in the FZ, A_b does not change as much because it is limited by a shallower h. Offshore, when H_{rms} is small and h is deeper a wider range of A_b can be realized. The result is a smaller spread of A_b and a tighter packing of bin averaged f_e (Figure 14). f_e appear to be relatively constant for A_b over the range of measured values. An average f_e of 6.3 is applied to predict wave transformation from the BZ to the FZ using the TG83 wave transformation model.

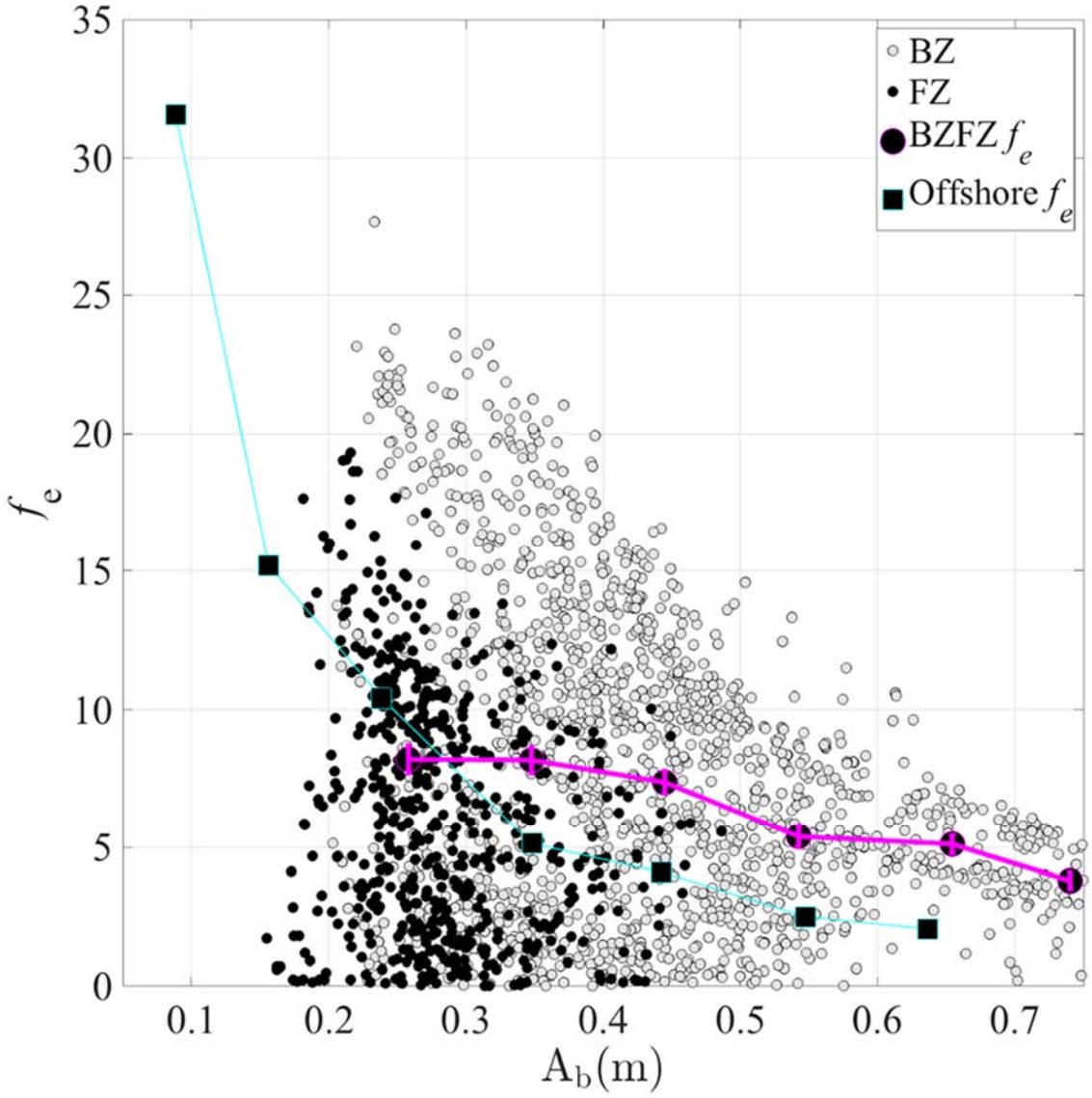

Figure 14. f_e as a function of A_b for the BZ (grey circles) and the FZ (black circles). Bin-averaged f_e for the BZ and FZ are plotted as larger black circles with magenta outlines. Magenta vertical lines represent 95% confidence intervals for bin-averaged f_e. Seaward of wave breaking bin-averaged f_e as a function of A_b are plotted as larger black squares with cyan outlines (Chapter II).

3. Dissipation in the BZ and FZ

Energy flux (F) was calculated at each of the stations in the BZ and on the FZ. Between BZ1 and BZ5, there is an average reduction of 96% in F that occurs in 94 m, which corresponds to an average 72% reduction in H_{rms} (Figure 11d, 15a). Between FZ1 and FZ6, there is an average reduction of 60% in F over 81 m. F across the FZ stations is tidally modulated where the largest change occurs at high tide (Figure 15b).

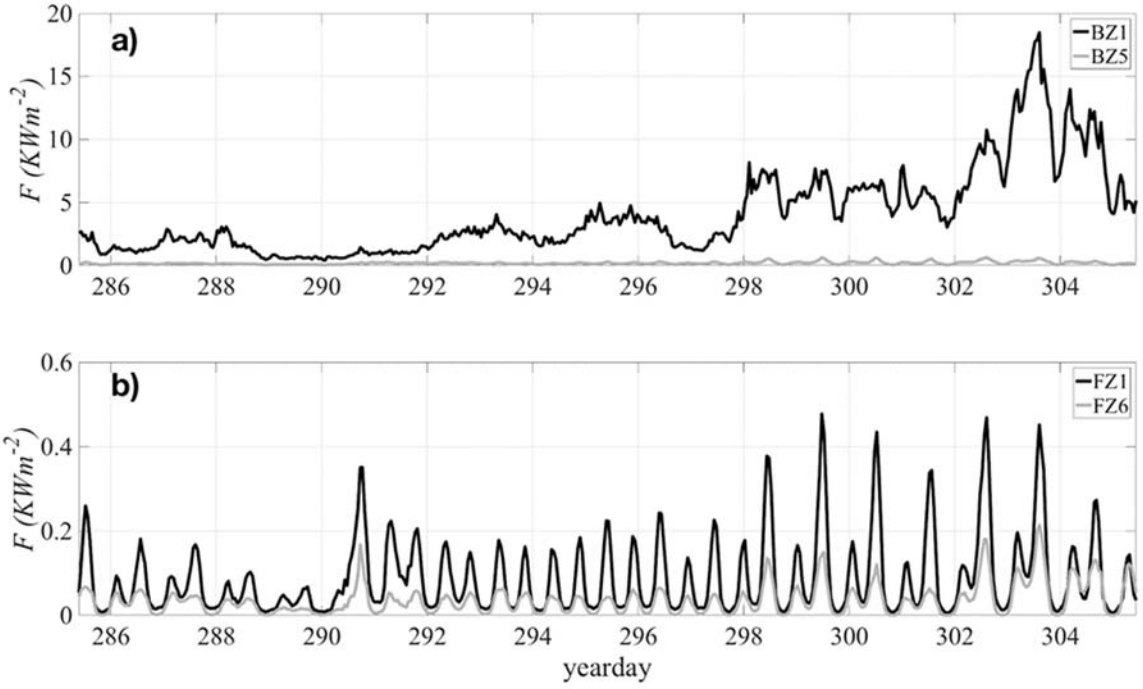

Figure 15. a) F at BZ1 (black line) and BZ5 (grey line); b) F at FZ1 (black line) and FZ6 (grey line).

D. DISCUSSION

1. Dissipation by Wave Breaking and Friction

Wave dissipation in the surf zone is the result of wave breaking and or bottom friction. In Chapter II wave transformation over the rocky reef at HMS seaward of wave breaking was examined. Significant energy dissipation due to bottom friction was attributed to the rough bottom with a measured bottom standard deviation of 0.9 m. The roughness of the bottom in the BZ and the FZ appear to be a similar scale in size of the features present as seen offshore through underwater visual inspections. Therefore, it is expected that both bottom friction and wave breaking dissipation will be important as the waves propagate across the nearshore into shallower water depths.

The TG83 model (14) with (19) and (22) describes wave transformation in the nearshore due to combined dissipation by wave breaking and bottom friction. The breaking wave dissipation formulation has the two free parameters, B and γ, that must be specified. It is assumed breaking waves are fully formed with B=1 and that $\gamma = 0.29$ as found earlier. The bottom friction dissipation formulation has one free parameter, f_e, that must be specified.

As an example, for stations BZ1 and BZ2, there was an average reduction of 55% in F (Figure 8a). The reduction in F is relatively independent of H_{rms}, but shows the largest reduction occurs at low tide (Figure 16a). Both wave breaking and bottom friction contributed to dissipation (Figure 16c). During small waves (H_{rms}<0.5 m), ε_f dominated ε_b indicative of BZ2 being mostly outside of wave breaking (Figure 16c). During moderate waves (0.5<H_{rms}<1) ε_f and ε_b contributed to ε (Figure 16c) suggesting BZ2 is inside of wave breaking part of the time. While during larger wave conditions (H_{rms}> 1 m), ε_b was most important indicative of these stations now being inside of wave breaking (Figure 8c). During the experiment, ε_b represented approximately 12% of the dissipation while the remaining 88% was represented by ε_f. When $H_{rms} \geq 1$m, ε_b is responsible for 76% dissipation.

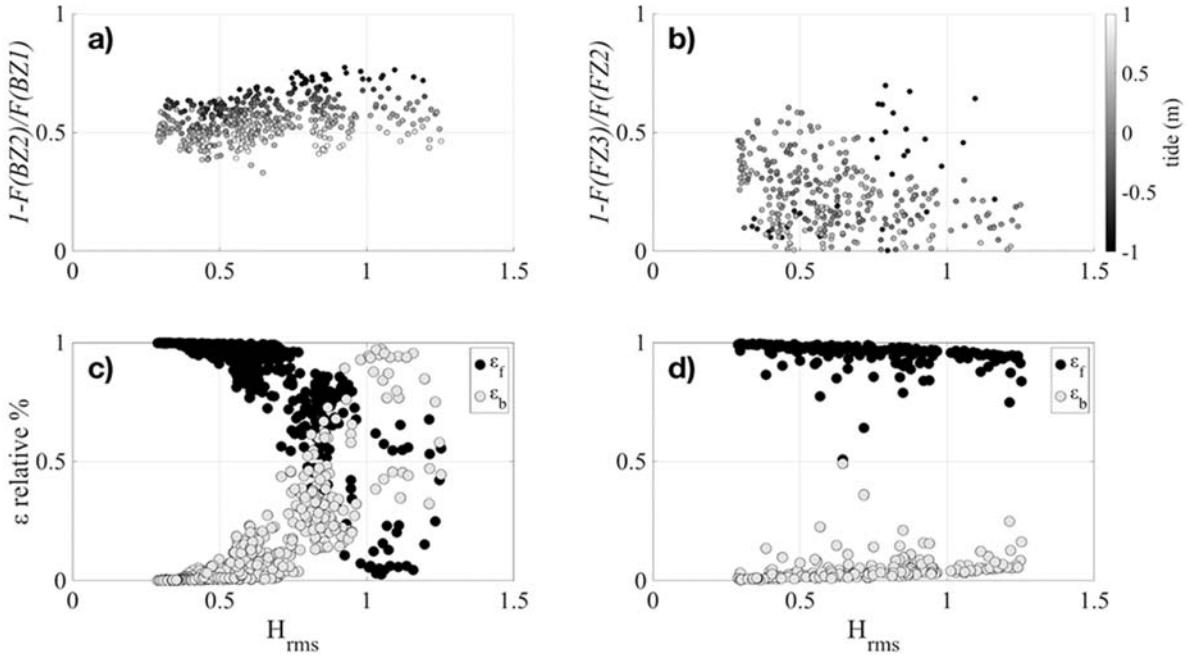

Figure 16. a and b) % reduction in F at BZ1 (FZ1) and BZ2 (FZ3) as a function of H_{rms} and tide; c and d) % contribution of ε_f (black dots) and ε_b(grey dots) to ε between BZ1 (FZ1) and BZ2 (FZ3) as a function of H_{rms}.

For the FZ there is a 24% reduction in F between FZ2 and FZ3 (Figure 16b). The reduction in F is independent of H_{rms} and tide. ε_b only contributes 4% to dissipation as waves are no longer breaking on the mild-sloping reef (Figure 16d). Owing to the lack of wave breaking and near zero contribution by ε_b, the wave transformation is described solely by ε_f.

Overall ε_f is the dominant dissipation process when $H_{rms} \leq 1$ m. When $H_{rms} > 1$ m, ε_b is the dominant process in BZ, but ε_f remains the dominant dissipative process in the FZ. Therefore, dissipation by bottom friction is important seaward of breaking (Chapter II), within breaking (BZ results) and shoreward of breaking along the reef (FZ results).

2. Analytical Model with Bottom Friction Dissipation Only

The analytical wave transformation model GTM with bottom friction dissipation only (31) is compared with measured $H_{rms}(h)$ across the BZ and the FZ (Figure 5b, c). In comparing $H_{rms}(h)$ in the BZ, the model is initialized with a depth-limited breaking value

of H_{rms}= 1.9m at h= 6.5m for γ= 0.29 and applied to a plane slope of 1/30 (Figure 3c). For FZ GTM was initialized using wave height and depth conditions at BZ3 on a plane bottom slope of 1/70.

The GTM model is in good agreement with bin averaged measured $H_{rms}(h)$ (cyan line, Figure 13c) suggesting that waves over the shallow reef are frictionally depth limited and that dissipation within this region is due to bottom friction. While all $H_{rms}(h)$ collapses to a non-linear shape, some of the data exceeds the frictional depth limitation set by GTM due to the irregularities in the bathymetry between stations. Applying GTM to the BZ in deeper depths and on a steeper slope is different as $H_{rms}(h)$ has more spread in the data (Figure 13b). In depths of 1.5 to 3.5 m GTM marks the depth limitation due to friction and the observed $H_{rms}(h)$ for these depths are at or below this limitation (Figure 13b). When $H_{rms}(h)$ is at the frictional limitation at these depths where the data are tightly packed and slightly non-linear (similar to FZ), dissipation of wave energy is solely a function of friction consistent with the findings in the FZ. For h>3.5, $H_{rms}(h)$ exceed the GTM limitation (cyan line in Figure 13b). This suggests that friction is not the limiting factor and that wave breaking is contributing, which has a larger limitation (magenta line in Figure 13b).

Model sensitivity to variations in H_{rms}, bottom slope and f_e are provided in Figure 17. Model sensitivity based on bottom slope indicates GTM becomes more linear as bottom slope increases (Figure 17b). These findings are consistent in the GTM results and the observed $H_{rms}(h)$ for shallow depths in the BZ as there is still a non-linearity in the data based on a 1/30 slope, but not nearly as non-linear as the FZ where slope was 1/70 (Figure 13b, c).

Lentz et al. (2016) independently derived an analytical solution for wave transformation due to bottom friction over a horizontal bed for shallow water waves that was earlier solved more generally for any h by Dean and Dalrymple (1984). They found agreement between their model and data of wave transformation over a coral reef for constant h.

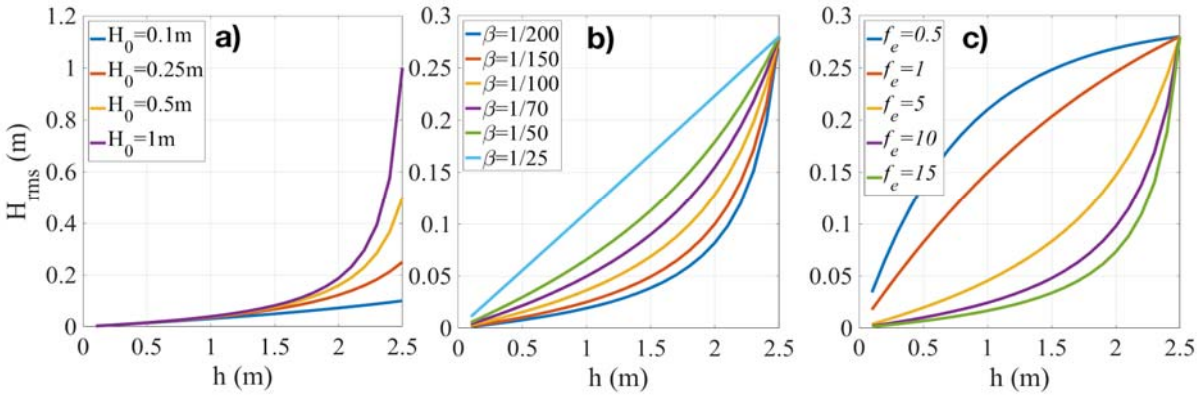

Figure 17. GTM model sensitivity analysis. a) GTM model sensitivity of H_{rms} transformation over the rocky reef for differing H_O for constant slope 1/100; b) Model sensitivity for varying bottom slope $tan\beta$ for constant bottom slope 1/100 and H_O= 0.25m; c) Model sensitivity for varying f_e for constant bottom slope 1/100 and H_O= 0.25m.

On the rocky reef, h is not constant (Figure 11c). The sensitivity of variable initial wave height finds the transformation more nonlinear for large wave heights with a faster initial decay (Figure 17a). The wave transformation for variable bottom slope with constant initial H_{rms} and f_e= 6.3 show an almost linear shape for a steep 1/25 slope becoming more nonlinear for gentler slopes (Figure 17b). Lastly, for varying f_e and constant initial H_{rms} and bottom slope= 1/100, wave transformation is monotonically decreasing for large values of f_e>2 approaching a similar decay rate for f_e>20 (Figure 17c). For smaller values of f_e<2, the wave transformation is convex. For f_e = 0, the exact solution is F=constant valid for any depth, which says wave heights grow as waves shoal and blows up as h approaches zero (Figure 16c).

3. Model Skill of TG83 on a Rocky Reef

Adopting an average f_e=6.3, $\gamma = 0.29$ and setting B=1, TG83 is applied from BZ1 to FZ6. TG83 was initialized at BZ1. The model skill was evaluated following Wilmott (1982):

$$Skill = 1 - \left[\frac{\Sigma\left(H_{rms,mod} - H_{rms,BZFZ}\right)^2}{\Sigma\left(\left|H_{rms,mod} - \overline{H_{rmsBZFZ}}\right| + \left|H_{rms,BZFZ} - \overline{H_{rms,BZFZ}}\right|\right)^2}\right] \qquad (33)$$

where subscripts mod represents the model and BZFZ represent the measurements. A skill=1 implies the model has perfectly predicted the observations and if skill is 0, there is no statistical prediction skill. TG83 performs well with $Skill \geq 0.9$ 90% of the time and $Skill \geq 0.8$ 99% of the time (Figure 18). $H_{rms,mod}$ trends to perform best when $H_{rms} \geq 1$m resulting in an average skill of 0.97 (Figure 18). The high skill suggests the spatial evaluation is relatively insensitive to using an average f_e. f_e has the greatest variability when the waves are small (small A_b in Figure 14), for which the skill is reduced (Figure 18).

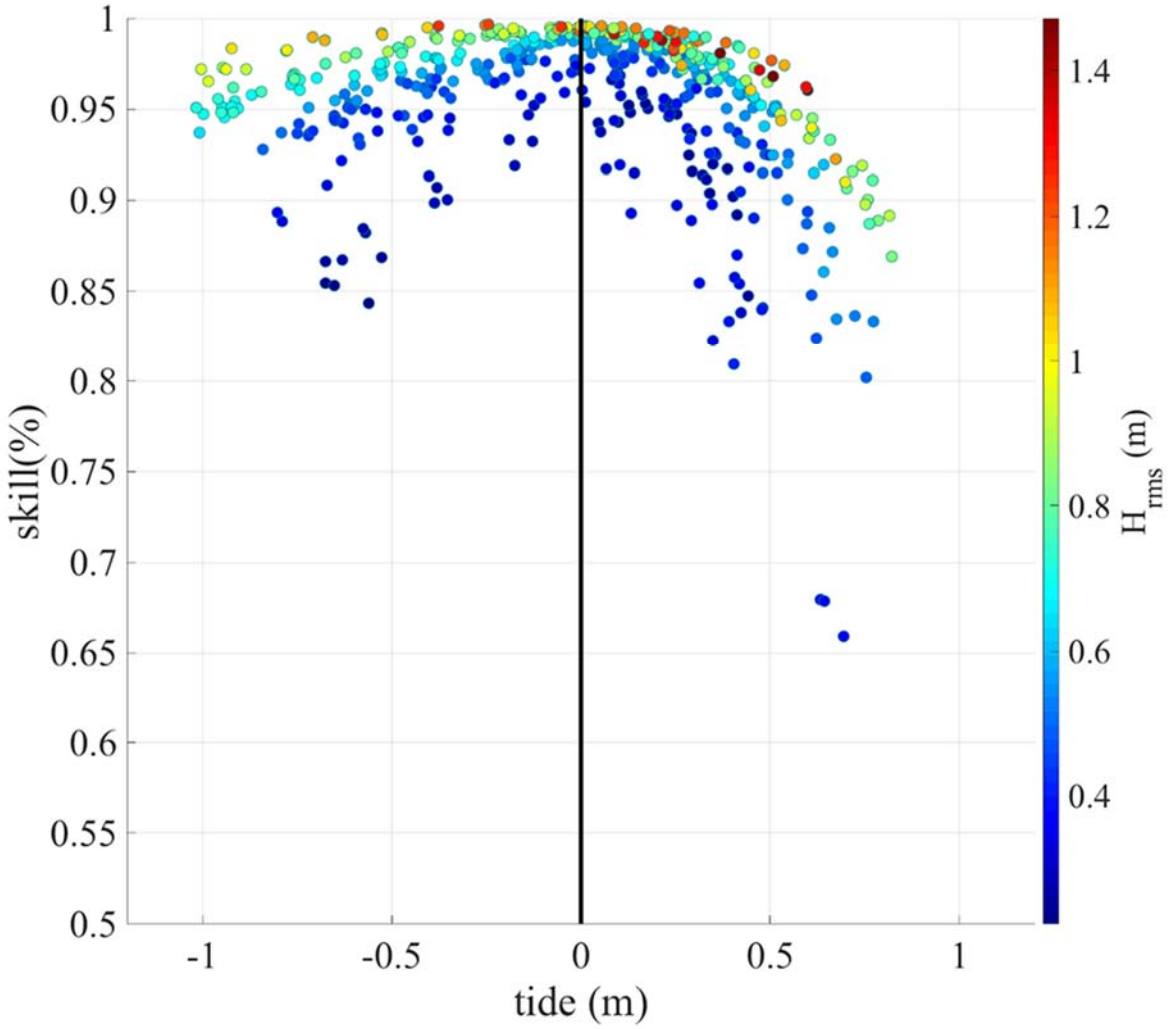

Figure 18. Model skill plotted as a function of tide and incident H_{rms} defined by the dot color. Black vertical line represents separation between high tide and low tide.

IV. CONCLUSIONS

In Chapter II results from two wave transformation experiments conducted on the rocky reef at Hopkins Marine Station, in the Monterey Bay found 28–36% of the energy dissipated in less than 140 m between 14 m to 7 m depth, outside of wave breaking. These findings suggest energy dissipation due to bottom friction is an important process on rocky shorelines influencing wave transformation.

Wave energy dissipation due to bottom friction is a function of the roughness of the ocean bottom, which controls the reduction in offshore F. A_b is comparable to σ_b for the rocky reef, indicating inertial forces are dominant (Yu et al. 2018). It is hypothesized that multiple scales contribute to the large values of f_e and $\langle \varepsilon_f \rangle$ presented here, but more research is required to confirm this. The standard deviation (σ_b) of the height elements was used to represent geometric roughness. Data sets containing measured roughness values were considered for comparison to the findings at the rocky reef. The rocky reef σ_b was 0.9 m compared with the coral reefs σ_b of 0.04-0.13 m, and with Type A rocky platforms σ_b 0.02-0.04 m. Large σ_b also corresponded to larger than expected mean f_e equal to 8.3 and 12.8 for experiment A and B. Until recent field research by Lentz et al. (2016); Monismith et al. (2015) and Rogers et al. (2016), large f_e were only seen in laboratories. f_e at the rocky shorelines are of the same order of magnitude of the aforementioned studies, but an order of magnitude larger than previous f_e on coral reefs presented by Lowe et al. (2005) and Monismith et al. (2013).

f_e was calculated numerically using an iterative forward-differencing scheme across the bottom profile. The optimized f_e were compared to $f_{e,midpoint}$ determined from the midpoint method that had nearly a 1:1 agreement for T = 9–11 s. Biases were present for T < 9 s and T>11 s, where the midpoint averages under predict by a factor of 2 for short period waves, and over predict by 25% for long period waves. In general, there is sensitivity between f_e and wave period (Figure 7). Additionally, from (8) it is seen that $\langle \varepsilon_f \rangle$ does not increase linearly, which is the assumption when applying the midpoint method. From (8),

this is not the case and the numerical method accounts for this sharp increase in $\langle \varepsilon_f \rangle$ with decreasing depth.

Empirical relationships (12) and (13) were developed between f_e, bottom roughness (σ_b), and orbital wave excursion amplitude, A_b, calculated based on H_{rms} and linear wave theory. Results from four experiments, one on rocky platforms, two on coral reefs and the rocky reef reported here, that span 4 orders of magnitude were used to develop a new formulation that deviates from previous empirical relationships over the range $0.01<\frac{A_b}{\sigma_b}<100$. The new power law empirical relationship solves for f_e based on wave and bathymetric measurements.

In Chapter III, nearshore wave transformation in water depths (h) less than 5 m at was examined through measurements and models by 1) evaluating observed H_{rms} as a function of h, $H_{rms}(h)$, for all measurement stations, 2) computing dissipation and relative contribution of wave breaking and bottom friction between station pairs, 3) deriving a bottom-friction only analytical model for a sloping bottom, and 4) testing the analytical model and the Thornton and Guza (1983) model, which includes dissipation by bottom friction and wave breaking. Similar to the offshore findings in Chapter II, dissipation by bottom friction inside of wave breaking is significant on a rocky reef owing to its increased bottom roughness, which correspondingly modifies the wave transformation.

For h>2 m, $H_{rms}(h)$ was found to modulate with the 2 m tide and offshore incident wave energy. Wave saturation by wave breaking was observed for largest waves located at the deepest stations. Excluding these extrema, $H_{rms}(h)$ was lower than the wave breaking saturation limit, $\gamma = 0.29$, suggesting bottom friction was also important. For $h<$ 2m, $H_{rms}(h)$ collapsed to a non-linear relationship that was modulated by the 2 m tide, was much lower than $\gamma = 0.29$, and solely controlled by bottom friction. These results differ from the typical linear $H_{rms}(h)$ relationship found on sandy beaches.

Large (>60%) reductions in energy fluxes were calculated over short distances. Total dissipation was estimated between station pairs. Dissipation by wave breaking was estimated using the measured $\gamma = 0.29$ and was subtracted from the total dissipation, where the residual represents dissipation by bottom friction. Bin-averaged wave energy

frictional factors, f_e, associated with dissipation by bottom friction were 3.8 to 8.2 with an average f_e of 6.3 and were inversely proportional to wave water particle excursions at the bed, A_b. These large f_e are consistent with f_e observed outside of wave breaking on rough bottoms (Lentz et al. 2016; Chapter II).

An analytical model for shallow-water wave transformation on a plane sloping bottom with bottom friction is derived and compared with observations. Using an average f_e of 6.3, the model compares well with observed $H_{rms}(h)$ for h<3 m suggesting that shallow-water wave transformation is controlled primarily by bottom friction. The non-linearity of $H_{rms}(h)$ is related to the incident wave height, bottom slope, and f_e. For h>3 m, dissipation by wave breaking also contributes, where the contribution increases with increasing offshore incident wave height. Applying the same parameters to the Thornton and Guza (1983) wave transformation model, which includes dissipation by breaking and bottom friction, when using the parameters $\gamma = 0.29$ and f_e= 6.3 compared well across the measurement array.

Wave transformation outside of wave breaking to the coast on a rough rocky reef is dominated by bottom friction. The results found on the rough rocky reef are consistent with the shallow water wave transformation on a rough coral reef (Lentz et al. 2016) A frictionally dominant environment as seen on the rough rocky reef, could be a contributing factor in enabling the diverse intertidal ecosystem to sustain and grow as wave-generated forces which are the leading cause of mortality are lessened in the rocky intertidal zone (Helmuth and Denny et al. 2003). Finally, one of the functions of a coral reef is coastal protection (Monismith et al. 2015). While the rocky reefs do not have a platform and lagoon setup like many coral reefs do (which have been shown to dissipate energy and serve to protect the coast), the reduction in offshore energy on the rocky reef is nearly identical to the reduction in energy due to friction on the coral reefs (Lowe et al. 2005; Monimsith et al. 2013; Monismith et al. 2015; Rogers et al. 2016; Lentz et al. 2016). This suggests that rocky reefs, also serve to protect their corresponding coasts as well.

THIS PAGE INTENTIONALLY LEFT BLANK

LIST OF REFERENCES

Baldock, T., P. Holmes, S. Bunker, and P. V. Weert, 1998: Cross-shore hydrodynamics within an unsaturated surf zone. *Coastal Engineering*, **34**, 173–196, https://doi.org/10.1016/s0378-3839(98)00017-9.

Bangold, R. A., 1946: Motion of waves in shallow water. Interaction between waves and sand bottoms. *Proceedings of the Royal Society of London. Series A. Mathematical and Physical Sciences*, **187**, 1–18, https://doi.org/10.1098/rspa.1946.0062.

Battjes, J. A., and J. P. F. M. Janssen, 1978: Energy loss and set-up due to breaking of random waves. *Coastal Engineering 1978*, https://doi.org/10.1061/9780872621909.034.

Bird, E., 2000: *Coastal Geomorphology: An Introduction*. John Wiley & Sons, 436 pp.

Britter, R. E., and S. R. Hanna, 2003: Flow and Dispersion in urban areas. *Annual Review Fluid Mechanics*, 469–496.

Broenkow, W. W., and L. Breaker, 2005: A 30 year history of tide and current measurements in Elkhorn Slough, California. *Moss Landing Marine Laboratories 2005*

Dean, R. G., and R. A. Dalrymple, 1984: *Water Wave Mechanics for Engineers and Scientists*. World Scientific, 353 pp.

Denny, M., J. Dairiki, and S. Distefano, 1992: Biological consequences of topography on wave-swept rocky shores: I. Enhancement of external fertilization. *The Biological Bulletin*, **183**, 220–232, https://doi.org/10.2307/1542209.

Denny, M. W., L. P. Miller, M. D. Stokes, L. J. H. Hunt, and B. S. T. Helmuth, 2003: Extreme water velocities: Topographical amplification of wave-induced flow in the surf zone of rocky shores. *Limnology and Oceanography*, **48**, 1–8, https://doi.org/10.4319/lo.2003.48.1.0001.

Dickson, W. S., T. H. C. Herbers, and E. B. Thornton, 1995: Wave reflection from breakwater. *Journal of Waterway, Port, Coastal, and Ocean Engineering*, **121**, 262–268, https://doi.org/10.1061/(asce)0733-950x(1995)121:5(262).

Eittreim, S. L., R. J. Anima, and A. J. Stevenson, 2002: Erratum to "Seafloor geology of the Monterey Bay area continental shelf." *Marine Geology*, **186**, 583, https://doi.org/10.1016/s0025-3227(02)00382-1.

Elgar, S., and R. T. Guza, 1985: Shoaling gravity waves: comparisons between field observations, linear theory, and a nonlinear model. *Journal of Fluid Mechanics*, **158**, 47–70, https://doi.org/10.1017/s0022112085002543.

Emery, K. O., and G. G. Kuhn, 1982: Sea cliffs: Their processes, profiles, and classification. *Geological Society of America Bulletin*, **93**, 644, https://doi.org/10.1130/0016-7606(1982)93<644:sctppa>2.0.co;2.

Fanning, J. T. 1877: *A Practical Treatise on Water-Supply Engineering.* Van Nostrand, 619 pp.

Grant, W. D., and O. S. Madsen, 1982: Movable bed roughness in unsteady oscillatory flow. *Journal of Geophysical Research*, **87**, 469, https://doi.org/10.1029/jc087ic01p00469.

Harris, D. L., H. E. Power, M. A. Kinsela, J. M. Webster, and A. Vila-Concejo, 2018: Variability of depth-limited waves in coral reef surf zones. *Estuarine, Coastal and Shelf Science*, **211**, 36–44, https://doi.org/10.1016/j.ecss.2018.06.010.

Harris, D. L., and A. Vila-Concejo, 2013: Wave transformation on a coral reef rubble platform. *Journal of Coastal Research*, **65**, 506–510, https://doi.org/10.2112/si65-086.1.

Helmuth, B., and M. W. Denny, 2003: Predicting wave exposure in the rocky intertidal zone: Do bigger waves always lead tolarger forces? *Limnology and Oceanography*, **48**, 1338–1345, https://doi.org/10.4319/lo.2003.48.3.1338.

Huntley, D. A., and M. A. Davidson, 1998: Estimating the directional spectrum of waves near a reflector. *Journal of Waterway, Port, Coastal, and Ocean Engineering*, **124**, 312–319, https://doi.org/10.1061/(asce)0733-950x(1998)124:6(312).

Hwang, L.-S., and D. Divoky, 1970: Breaking Wave Setup And Decay On Gentle Slopes. *Coastal Engineering Proceedings*, **1**, 23, https://doi.org/10.9753/icce.v12.23.

Iversen, H. W., 1952: Laboratory study of breakers. *Gravity waves*.

Janssen, T., and J. Battjes, 2007: A note on wave energy dissipation over steep beaches. *Coastal Engineering*, **54**, 711–716, https://doi.org/10.1016/j.coastaleng.2007.05.006.

Jimenez, J., 2004: Turbulent Flows Over Rough Walls. *Annual Review of Fluid Mechanics*, **36**, 173–196, https://doi.org/10.1146/annurev.fluid.36.050802.122103.

Jonsson, I. G., 1966: Wave boundary layers and friction factors. *Coastal Engineering 1966*, https://doi.org/10.1061/9780872620087.010.

Kench, P. S., and R. W. Brander, 2006: Wave processes on coral reef flats: Implications for reef geomorphology using Australian case studies. *Journal of Coastal Research*, **221**, 209–223, https://doi.org/10.2112/05a-0016.1.

Kennedy, D. M., and J. G. Beban, 2005: Shore platform morphology on a rapidly uplifting coast, Wellington, New Zealand. *Earth Surface Processes and Landforms*, **30**, 823–832, doi:10.1002/esp.1192.

Kirk, R. M., 1977: Rates and forms of erosion on intertidal platforms at Kaikoura Peninsula, South Island, New Zealand. *New Zealand Journal of Geology and Geophysics*, **20**, 571–613, https://doi.org/10.1080/00288306.1977.10427603.

Koehl, M.A.R. and Powell, T.M., 1994: Turbulent transport of larvae near wave-swept rocky shores: does water motion overwhelm larval sinking. *Reproduction and development of marine invertebrates. Johns Hopkins University Press, Baltimore*, pp.261-274.

LeMehaute, B., 1962: On non-saturated breakers and the wave run-up, paper presented at 8th International conference on coastal; engineering. American Society of Civil Engineers, Mexico City.

Lentz, S. J., J. H. Churchill, K. A. Davis, J. T. Farrar, J. Pineda, and V. Starczak, 2016: The characteristics and dynamics of wave-driven flow across a platform coral reef in the Red Sea. *Journal of Geophysical Research: Oceans*, **121**, 1360–1376, https://doi.org/10.1002/2015jc011141.

Lippmann, T., A. Brookins, and E. Thornton, 1996: Wave energy transformation on natural profiles. *Coastal Engineering*, **27**, 1–20, https://doi.org/10.1016/0378-3839(95)00036-4.

Lowe, R. J., J. L. Falter, M. D. Bandet, G. Pawlak, M. J. Atkinson, S. G. Monismith, and J. R. Koseff, 2005: Spectral wave dissipation over a barrier reef. *Journal of Geophysical Research*, **110**, https://doi.org/10.1029/2004jc002711.

Lowe, R. J., J. L. Falter, S. G. Monismith, and M. J. Atkinson, 2009: Wave-Driven Circulation of a Coastal Reef–Lagoon System. *Journal of Physical Oceanography*, **39**, 873–893, https://doi.org/10.1175/2008jpo3958.1.

Marshall, R. R. J., and W. J. Stephenson, 2011: The morphodynamics of shore platforms in a micro-tidal setting: Interactions between waves and morphology. *Marine Geology*, **288**, 18–31, https://doi.org/10.1016/j.margeo.2011.06.007.

Masselink, G., and B. Hegge, 1995: Morphodynamics of meso- and macrotidal beaches: examples from central Queensland, Australia. *Marine Geology*, **129**, 1–23, https://doi.org/10.1016/0025-3227(95)00104-2.

Miche, M., 1951: Le Pouvoir Réfléchissant des Ouvrages Maritimes Exposes a l' Action de la Houle Annals des Ponts et Chaussess. *121e nene*, 285–319.

Mirfenderesk, H., and I. R. Young, 2003: Direct measurements of the bottom friction factor beneath surface gravity waves. *Applied Ocean Research*, **25**, 269–287, https://doi.org/10.1016/j.apor.2004.02.002.

Monismith, S. G., 2007: Hydrodynamics of Coral Reefs. *Annual Review of Fluid Mechanics*, 37–55, https://doi.org/10.1146/annurev.fluid.38.050304.092125.

Monismith, S. G., L. M. M. Herdman, S. Ahmerkamp, and J. L. Hench, 2013: Wave Transformation and Wave-Driven Flow across a Steep Coral Reef. *Journal of Physical Oceanography*, **43**, 1356–1379, https://doi.org/10.1175/jpo-d-12-0164.1.

Monismith, S. G., J. S. Rogers, D. Koweek, and R. B. Dunbar, 2015: Frictional wave dissipation on a remarkably rough reef. *Geophysical Research Letters*, **42**, 4063–4071, https://doi.org/10.1002/2015gl063804.

Myrhaug, D., L. E. Holmedal, R. R. Simons, and R. D. Maciver, 2001: Bottom friction in random waves plus current flow. *Coastal Engineering*, **43**, 75–92, https://doi.org/10.1016/s0378-3839(01)00007-2.

Nelson, R., 1996: Hydraulic roughness of coral reef platforms. *Applied Ocean Research*, **18**, 265–274, https://doi.org/10.1016/s0141-1187(97)00006-0.

Nield, J. M., and Coauthors, 2013: Estimating aerodynamic roughness over complex surface terrain. *Journal of Geophysical Research: Atmospheres*, **118**, https://doi.org/10.1002/2013jd020632.

Nielsen, P., 1992: *Coastal Bottom Boundary Layers and Sediment Transport*. World Scientific.

Péquignet, A.-C., J. M. Becker, M. A. Merrifield, and S. J. Boc, 2011: The dissipation of wind wave energy across a fringing reef at Ipan, Guam. *Coral Reefs*, **30**, 71–82, https://doi.org/10.1007/s00338-011-0719-5.

Poate, T., G. Masselink, M. J. Austin, M. Dickson, and R. Mccall, 2018: The Role of Bed Roughness in Wave Transformation Across Sloping Rock Shore Platforms. *Journal of Geophysical Research: Earth Surface*, **123**, 97–123, https://doi.org/10.1002/2017jf004277.

Raubenheimer, B., R. T. Guza, and S. Elgar, 1996: Wave transformation across the inner surf zone. *Journal of Geophysical Research: Oceans*, **101**, 25589–25597, https://doi.org/10.1029/96jc02433.

Raupach, M. R., R. A. Antonia, and S. Rajagopalan, 1991: Rough-Wall Turbulent Boundary Layers. *Applied Mechanics Reviews*, **44**, 1, https://doi.org/10.1115/1.3119492.

Rogers, J. S., S. G. Monismith, D. A. Koweek, and R. B. Dunbar, 2016: Wave dynamics of a Pacific Atoll with high frictional effects. *Journal of Geophysical Research: Oceans*, **121**, 350–367, https://doi.org/10.1002/2015jc011170.

Ruessink, B., D. Walstra, and H. Southgate, 2003: Calibration and verification of a parametric wave model on barred beaches. *Coastal Engineering*, **48**, 139–149, https://doi.org/:10.1016/s0378-3839(03)00023-1.

Sallenger, A. H., and R. A. Hollman, 1985: Setup and swash on a natural beach. *Journal of Geophysical Research*, **90**, 945, https://doi.org/10.1029/jc090ic01p00945.

Soulsby, R., 1997: *Dynamics of Marine Sands*. Thomas Telford, 208 pp.

Stoker, J. J., 1957: *Water Waves*. Interscience, 567 pp.

Storlazzi, C., and M. Field, 2000: Sediment distribution and transport along a rocky, embayed coast: Monterey Peninsula and Carmel Bay, California. *Marine Geology*, **170**, 289–316, https://doi.org/10.1016/s0025-3227(00)00100-6.

Sunamura, T., 1992: *Geomorphology of rocky coasts*. Wiley, 302 pp.

Thornton, E. B., and R. T. Guza, 1983: Transformation of wave height distribution. *Journal of Geophysical Research*, **88**, 5925, https://doi.org/10.1029/jc088ic10p05925.

Thornton, E. B., and R. T. Guza, 1986: Surf Zone Longshore Currents and Random Waves: Field Data and Models. *Journal of* Physical *Oceanography*, **16**, 1165–1178, https://doi.org/10.1175/1520-0485(1986)016<1165:szlcar>2.0.co;2.

Trenhaile, A. S., 2002: Rock coasts, with particular emphasis on shore platforms. *Geomorphology*, **48**, 7–22, https://doi.org/10.1016/s0169-555x(02)00173-3.

Trowbridge, C. D., 2004: Emerging associations on marine rocky shores: specialist herbivores on introduced macroalgae. *Journal of Animal Ecology*, **73**, 294–308, https://doi.org/10.1111/j.0021-8790.2004.00808.x.

Willmott, C. J., 1982: Some Comments on the Evaluation of Model Performance. *Bulletin of the American Meteorological Society*, **63**, 1309–1313, https://doi.org/10.1175/1520-0477(1982)063<1309:scoteo>2.0.co;2.

Young, I. R., 1989: Wave transformation over coral reefs. *Journal of Geophysical Research*, **94**, 9779, https://doi.org/10.1029/jc094ic07p09779.

Yu, X., J. H. Rosman, and J. L. Hench, 2018: Interactions Of Waves With Idealized High-Relief Bottom Roughness. *Coastal Engineering Proceedings*, **1**, 57, https://doi.org/10.9753/icce.v36.waves.57.

INITIAL DISTRIBUTION LIST

1. Defense Technical Information Center
   Ft. Belvoir, Virginia

2. Dudley Knox Library
   Naval Postgraduate School
   Monterey, California